Supporting Information

Emergence of Nonlinear Optical Activity by Incorporation of a Linker Carrying the *p*-Nitroaniline Motif in MIL-53 Frameworks

Karen Markey,[a†] Martin Krüger,[b†] Tomasz Seidler,[c,d†] Helge Reinsch,[b] Thierry Verbiest,[e] Dirk E. De Vos,[a] Benoît Champagne,[d] Norbert Stock[b] and Monique A. van der Veen[f]

a. Centre for Surface Chemistry and Catalysis, Faculty of Bioscience Engineering, University of Leuven, Leuven, Belgium.
b. Institut für Anorganische Chemie, Christian-Albrechts-Universität zu Kiel, Kiel, Germany.
c. K. Gumiński Department of Theoretical Chemistry, Jagiellonian University, Romana Ingardena 3, 30-060 Kraków, Poland.
d. Unité de Chimie Physique Théorique et Structurale, University of Namur, 5000 Namur, Belgium.
e. Molecular Imaging and Photonics, KU Leuven – University of Leuven, 3001 Leuven, Belgium.
f. Catalysis Engineering, TU Delft, 2628 Delft, The Netherlands.
† K. Markey,M. Krüger and T. Seidler contributed equally.

Contents

Linker synthesis 2
MOF Synthesis 6
XRD patterns and refinements 14
TG curves and elementary analysis 20
SEM images 23
NMR spectra 27
Sorption experiments 29
SHG microscopy 31
Calculation of $\langle d_{eff} \rangle$ values 33
Ab initio calculations 34
Estimation of the transmittance of 400 nm light through MIL-53(Al)-NH_2-NO_2 crystals 40
UV-vis spectrum 42
SHG of MIL-53(Al)-NH_2/NO_2 (1) as a function of temperature 43
Bibliography 44

Linker synthesis

2-Amino-5-nitroterephthalic acid (H_2BDC-NH_2/NO_2): The synthesis was accomplished by following the literature procedure published by Skibo et al. The reaction scheme is shown in **Figure S1**.

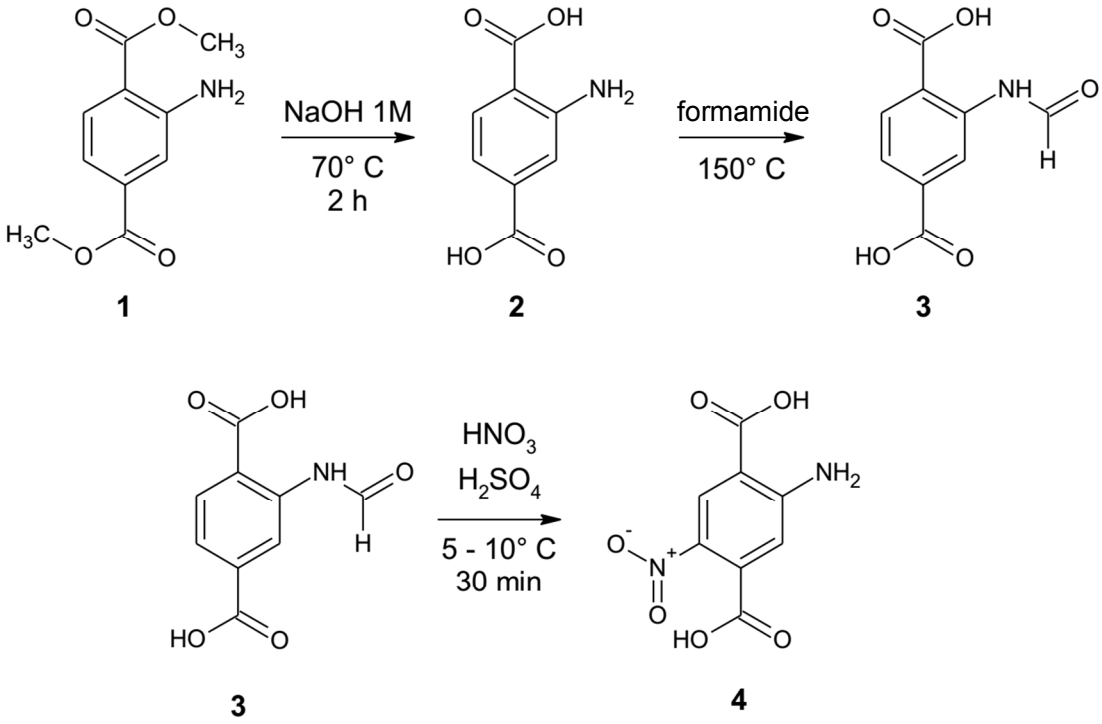

Figure S1. Reaction scheme for the synthesis of 2-amino-5-nitroterephthalic acid (H_2BDC-NH_2/NO_2).

Step 1: A mixture of 87 g (416 mmol) of dimethyl aminoterephthalate and 800 mL of a 1M NaOH solution was heated in a 1 L flask to 70 °C until the solid was dissolved completely. After cooling down to room temperature conc. HCl was added until a yellow solid precipitated which was filtered and washed with water.

Yield: 67 g (370 mmol, 89%)

^{1}H-NMR: (200 MHz, DMSO-D6, 300 K): δ [ppm]: 7.77 (1H, d, J = 8.3 Hz, H3), 7.39 (1H, d, J = 1.4 Hz, H1), 7.02 (1H, dd, J = 8.3 Hz, J = 1.6 Hz, H2).

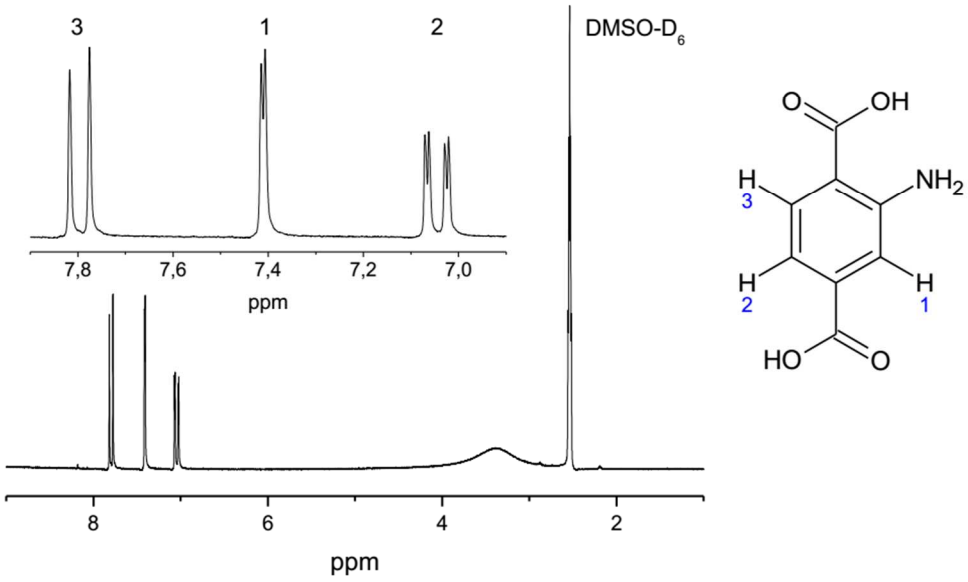

Figure S2. ^{1}H-NMR spectrum of aminoterephthalic acid.

Step 2: A suspension of 20.8 g aminoterephthalic acid (114 mmol) and 100 mL formamide was heated rapidly to 150 °C until the solid was dissolved. During cooling down to room temperature a brown solid precipitated which was filtered of and dissolved in a saturated aqueous Na(HCO_3) solution. While acidifying this solution with conc. acetic acid a white solid precipitated which was filtered off, washed with water and dried completely.

Yield: 9.7 g (53 mmol, 48%)

^{1}H-NMR: (200 MHz, DMSO-D6, 300 K): δ [ppm]: 9.1 (1H, s H1), 8.54 (1H, s H2), 8.07 (1H, d, J = 8.2 Hz, H4), 7.69 (1H dd, J = 8.2 Hz, J = 1.7 Hz, H3)

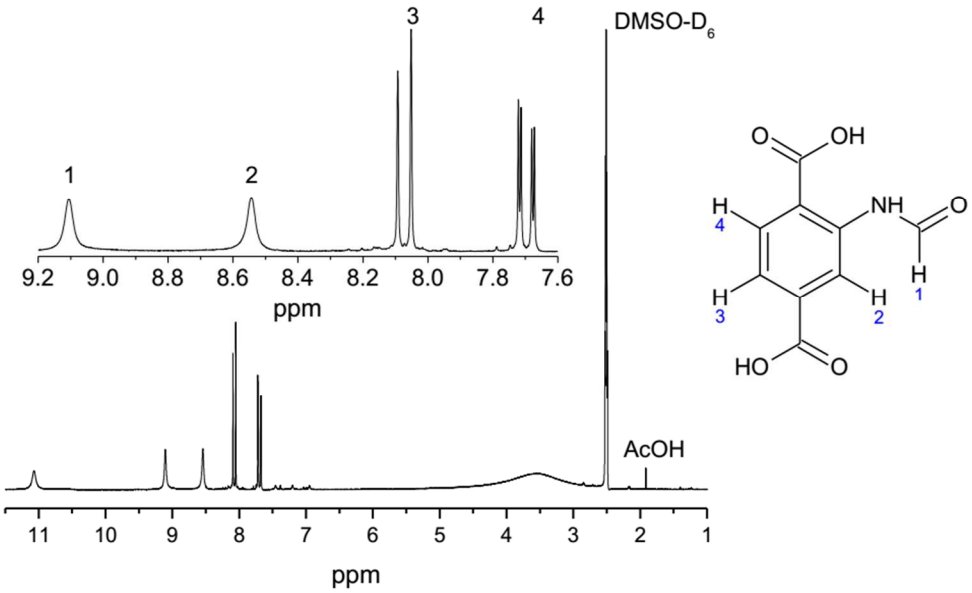

Figure S3. [1]H-NMR spectrum of formamidoterephthalic acid.

Step 3: To 20 mL of fuming nitric acid, cooled in an ice bath, 5.1 g (24 mmol) of formamidoterephthalic acid was added under stirring. To this suspension 10 mL of conc. sulfuric acid, which was also cooled in an ice bath, was added slowly within 15-20 minutes keeping the temperature between 5-10°C. After addition, the solid was dissolved and the solution was purred on 100 g of ice and stored in a refrigerator overnight. The precipitated solid was filtered off and recrystallized from hot water. Orange-brown crystals were obtained.

Yield: 1.5 g (6.6 mmol, 27%)

[1]H-NMR: (200 MHz, DMSO-D6, 300 K): δ [ppm]: 8.49 (1H, s, H1), 6.89 (1H, s, H2).

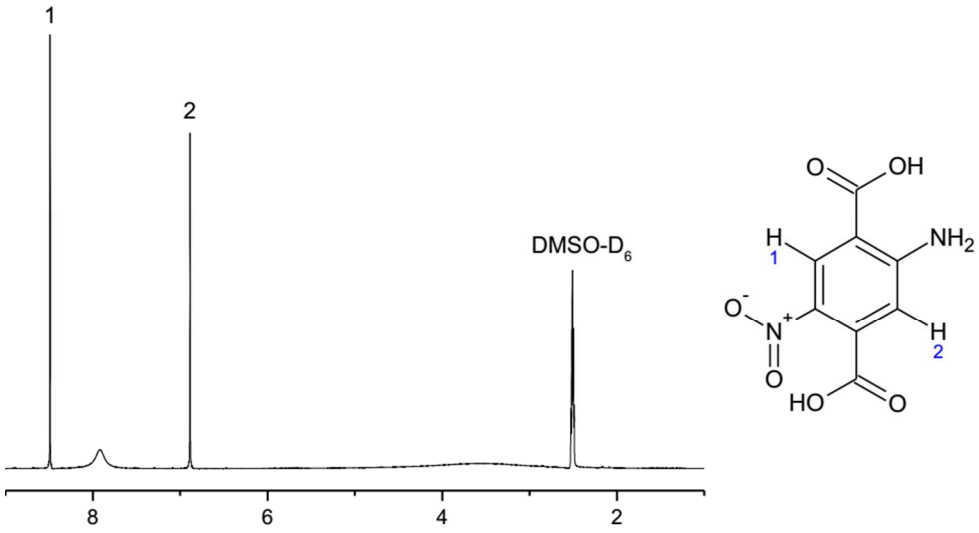

Figure S4. [1]H-NMR spectrum of 2-amino-5-nitroterephthalic acid (H_2BDC-NH_2/NO_2) measured in DMSO-D6.

[1]H-NMR: (200 MHz, NaOD/D2O, 300 K): δ [ppm]: 8.36 (1H, s, H1), 6.41 (1H, s, H2).

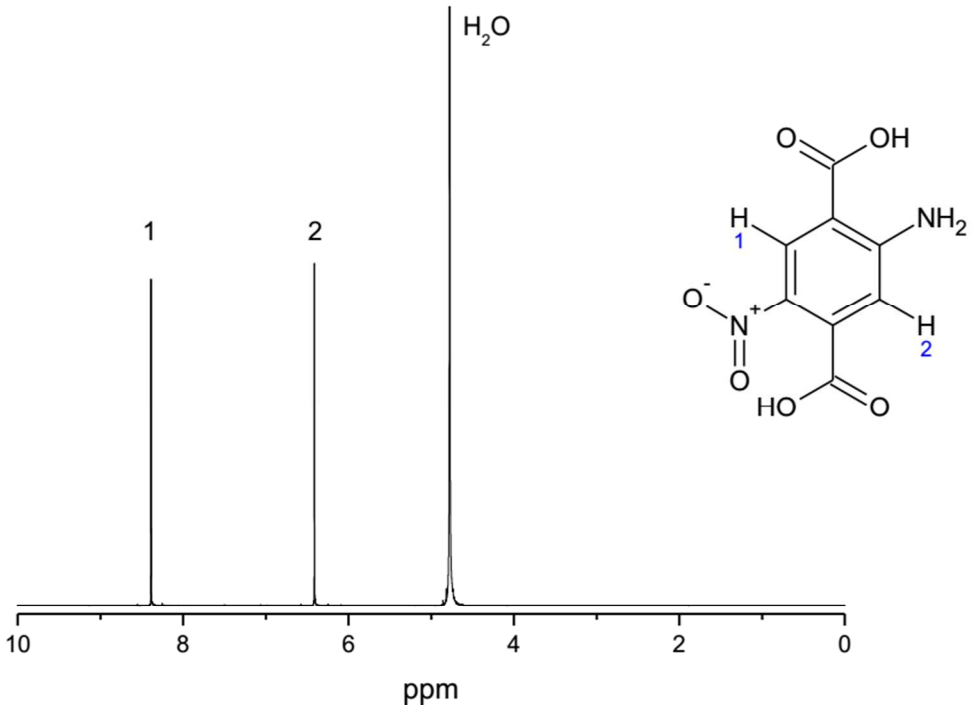

Figure S5. ^{1}H-NMR spectrum of 2-amino-5-nitroterephthalic acid ($H_2BDC\text{-}NH_2/NO_2$) measured in 5% NaOD/D_2O.

MOF Synthesis

Table S1. Molar ratios and exact amounts of the reactants employed in the HT experiments for MIL-53(Al)-NH_2/NO_2.

metal source	No.	equivalent linker	equivalent Al^{3+}	additive [µL/mg]	linker [mg]	Al^{3+} [µL/mg]	V H_2O [µL]	V DMF [µL]	temperature program
2 M $AlCl_3 \cdot 6H_2O$ in H_2O	1	2	1	0	20.0	22.1	477.9	0.0	1h/12h\1h 160°C
	2	2	2	0	20.0	44.2	455.8	0.0	
	3	2	3	0	20.0	66.4	433.6	0.0	
	4	3	2	0	30.0	44.2	455.8	0.0	
	5	3	3	0	30.0	66.4	433.6	0.0	
	6	3	4	0	30.0	88.5	411.5	0.0	
2 M $Al(NO_3)_3 \cdot 9H_2O$ in H_2O	7	2	1	0	20.0	22.1	477.9	0.0	
	8	2	2	0	20.0	44.2	455.8	0.0	
	9	2	3	0	20.0	66.4	433.6	0.0	
	10	3	2	0	30.0	44.2	455.8	0.0	
	11	3	3	0	30.0	66.4	433.6	0.0	
	12	3	4	0	30.0	88.5	411.5	0.0	
2 M $AlCl_3 \cdot 6H_2O$ in H_2O	13	1	1	0	10.0	22.1	127.9	0.0	1h/12h\1h 180°C
	14	1	2	0	10.0	44.2	105.8	0.0	
	15	1	4	0	10.0	88.5	61.5	0.0	
	16	2	0.5	0	20.0	11.1	138.9	0.0	
	17	2	1	0	20.0	22.1	127.9	0.0	
	18	2	2	0	20.0	44.2	105.8	0.0	
	19	2	2	0	20.0	44.2	105.8	0.0	
	20	2	2	0	20.0	44.2	85.8	20.0	
	21	2	2	0	20.0	44.2	65.8	40.0	
	22	2	2	0	20.0	44.2	45.8	60.0	
	23	2	2	0	20.0	44.2	25.8	80.0	
	24	2	2	0	20.0	44.2	5.8	100.0	
	25	1	1	0	10.0	22.1	277.9	200.0	
	26	1	2	0	10.0	44.2	255.8	200.0	
	27	1	3	0	10.0	66.4	233.6	200.0	
	28	2	0.5	0	20.0	11.1	288.9	200.0	
	29	2	1	0	20.0	22.1	277.9	200.0	
	30	2	2	0	20.0	44.2	255.8	200.0	
$AlCl_3 \cdot 6H_2O$	31	1	1	0	10.0	10.7	300.0	200.0	
	32	1	2	0	10.0	21.4	300.0	200.0	
	33	1	3	0	10.0	32.0	300.0	200.0	
	34	2	0.5	0	20.0	5.3	300.0	200.0	
	35	2	1	0	20.0	10.7	300.0	200.0	
	36	2	2	0	20.0	21.4	300.0	200.0	

				2M NaOH [µL]					
	37	2	2	4.4	20.0	21.4	295.6	200.0	
	38	2	2	8.8	20.0	21.4	291.2	200.0	
	39	2	2	13.3	20.0	21.4	286.7	200.0	
	40	2	2	17.7	20.0	21.4	282.3	200.0	
	41	2	2	22.1	20.0	21.4	277.9	200.0	
	42	2	2	26.5	20.0	21.4	273.5	200.0	
2 M $AlCl_3$ ·$6H_2O$ in H_2O	43	1	1	0	10.0	22.1	67.9	60.0	
	44	1	2	0	10.0	44.2	45.8	60.0	
	45	1	3	0	10.0	66.4	23.6	60.0	
	46	2	0.5	0	20.0	11.1	78.9	60.0	
	47	2	1	0	20.0	22.1	67.9	60.0	
	48	2	2	0	20.0	44.2	45.8	60.0	
$AlCl_3$ ·$6H_2O$	49	1	1	10	10.0	10.7	90.0	60.0	
	50	1	2	10	10.0	21.4	90.0	60.0	
	51	1	3	10	10.0	32.0	90.0	60.0	
	52	2	0.5	10	20.0	5.3	90.0	60.0	
	53	2	1	10	20.0	10.7	90.0	60.0	
	54	2	2	10	20.0	21.4	90.0	60.0	
	55	2	2	8.8	20.0	21.4	81.2	60.0	
	56	2	2	17.7	20.0	21.4	72.3	60.0	
	57	2	2	26.5	20.0	21.4	63.5	60.0	
	58	2	2	35.4	20.0	21.4	54.6	60.0	
	59	2	2	44.2	20.0	21.4	45.8	60.0	
	60	2	2	53.1	20.0	21.4	36.9	60.0	
2 M $AlCl_3$ ·$6H_2O$ in H_2O	61	2	2	13.3	20.0	44.2	32.5	60.0	1h/12h\1h 150°C
	62	2	2	22.1	20.0	44.2	23.6	60.0	
	63	3	3	0.0	30.0	66.4	23.6	60.0	
	64	3	3	17.7	30.0	66.4	5.9	60.0	
$AlCl_3$ ·$6H_2O$	65	3	3	26.5	30.0	32.0	63.5	60.0	
	66	3	3	35.4	30.0	32.0	54.6	60.0	
2 M $AlCl_3$ ·$6H_2O$ in H_2O	67	2	2	13.3	20.0	44.2	32.5	60.0	1h/36h\1h 150°C
	68	2	2	22.1	20.0	44.2	23.6	60.0	
	69	3	3	0.0	30.0	66.4	23.6	60.0	
	70	3	3	17.7	30.0	66.4	5.9	60.0	
$AlCl_3$ ·$6H_2O$	71	3	3	26.5	30.0	32.0	63.5	60.0	
	72	3	3	35.4	30.0	32.0	54.6	60.0	

Table S2. Molar ratios and exact amounts of the reactants employed in the HT experiments for MIL-53(Al)-NH_2/NO_2 (2).

metal source	No.	equivalent linker	equivalent Al^{3+}	additive [µL/mg]	linker [mg]	Al^{3+} [µL/mg]	V H_2O [µL]	V EtOH [µL]	temperature program
$AlCl_3 \cdot 6H_2O$	1	2	2	0	20.0	21.4	125.0	25.0	1h/36h\1h 150°C
	2	2	2	0	20.0	21.4	100.0	50.0	
	3	2	2	0	20.0	21.4	75.0	75.0	
	4	2	2	0	20.0	21.4	50.0	100.0	
	5	2	2	0	20.0	21.4	25.0	125.0	
	6	2	2	0	20.0	21.4	0.0	150.0	
	7	2	2	0	20.0	21.4	10.0	140.0	
	8	2	2	0	20.0	21.4	15.0	135.0	
	9	2	2	0	20.0	21.4	20.0	130.0	
	10	2	2	0	20.0	21.4	25.0	125.0	
	11	2	2	0	20.0	21.4	30.0	120.0	
	12	2	2	0	20.0	21.4	35.0	115.0	

Table S3. Molar ratios and exact amounts of the reactants employed in the HT experiments for MIL-53(Ga)-NH_2/NO_2.

metal source	No.	equivalent linker	equivalent Ga^{3+}	additive [µL/mg]	linker [mg]	Ga^{3+} [µL/mg]	V EtOH [µL]	V H_2O [µL]	temperature program
2M $Ga(NO_3)_3 \cdot H_2O$ in H_2O	1	1	0.5	0	10.0	11.1	10.0	128.9	1h/36h\1h 150°C
	2	1	1	0	10.0	22.1	10.0	117.9	
	3	1	2	0	10.0	44.2	10.0	95.8	
	4	2	1	0	20.0	22.1	10.0	117.9	
	5	2	2	0	20.0	44.2	10.0	95.8	
	6	2	4	0	20.0	88.5	10.0	51.5	
	7	1	0.5	0	10.0	11.1	20.0	118.9	
	8	1	1	0	10.0	22.1	20.0	107.9	
	9	1	2	0	10.0	44.2	20.0	85.8	
	10	2	1	0	20.0	22.1	20.0	107.9	
	11	2	2	0	20.0	44.2	20.0	85.8	
	12	2	4	0	20.0	88.5	20.0	41.5	
	13	1	0.5	0	10.0	11.1	40.0	98.9	8h/16h\4h 150°C
	14	1	1	0	10.0	22.1	40.0	87.9	
	15	1	2	0	10.0	44.2	40.0	65.8	
	16	2	1	0	20.0	22.1	40.0	87.9	
	17	2	2	0	20.0	44.2	40.0	65.8	
	18	2	4	0	20.0	88.5	40.0	21.5	
	19	1	0.5	0	10.0	11.1	60.0	78.9	
	20	1	1	0	10.0	22.1	60.0	67.9	
	21	1	2	0	10.0	44.2	60.0	45.8	
	22	2	1	0	20.0	22.1	60.0	67.9	
	23	2	2	0	20.0	44.2	60.0	45.8	

	24	2	4	0	20.0	88.5	60.0	1.5	
	25	2	2	0	20.0	44.2	10.0	95.8	24h/24h\12h 150°C
	26	2	2	0	20.0	44.2	20.0	85.8	
	27	2	2	0	20.0	44.2	50.0	55.8	
	28	2	2	0	20.0	44.2	60.0	45.8	
	29	2	2	0	20.0	44.2	85.0	20.8	
	30	2	2	0	20.0	44.2	100.0	5.8	
	31	2	2	0	20.0	44.2	10.0	95.8	4h/16h\8h 150°C
	32	2	2	0	20.0	44.2	20.0	85.8	
	33	2	2	0	20.0	44.2	50.0	55.8	
	34	2	2	0	20.0	44.2	60.0	45.8	
	35	2	2	0	20.0	44.2	85.0	20.8	
	36	2	2	0	20.0	44.2	100.0	5.8	
	37	2	2	0	20.0	44.2	10.0	95.8	12h/36h\12h 130°C
	38	2	2	0	20.0	44.2	60.0	45.8	
	39	2	2	0	20.0	44.2	100.0	5.8	
	40	2	1	0	20.0	22.1	20.0	107.9	
	41	2	2	0	20.0	44.2	20.0	85.8	
	42	2	4	0	20.0	88.5	20.0	41.5	
	43	2	2	0	20.0	44.2	30.0	225.8	
	44	2	2	0	20.0	44.2	150.0	105.8	
	45	2	2	0	20.0	44.2	250.0	5.8	
	46	2	1	0	20.0	22.1	50.0	227.9	
	47	2	2	0	20.0	44.2	50.0	205.8	
	48	2	4	0	20.0	88.5	50.0	161.5	
								V DMF [µL]	
	49	2	2	0	20.0	44.2	10.0	95.8	
	50	2	2	0	20.0	44.2	60.0	45.8	
	51	2	2	0	20.0	44.2	100.0	5.8	
	52	2	1	0	20.0	22.1	20.0	107.9	
	53	2	2	0	20.0	44.2	20.0	85.8	
	54	2	4	0	20.0	88.5	20.0	41.5	
	55	2	2	0	20.0	44.2	30.0	225.8	
	56	2	2	0	20.0	44.2	150.0	105.8	
	57	2	2	0	20.0	44.2	250.0	5.8	
	58	2	1	0	20.0	22.1	50.0	227.9	
	59	2	2	0	20.0	44.2	50.0	205.8	
	60	2	4	0	20.0	88.5	50.0	161.5	
				2M NaOH [µL]			V H_2O [µL]		1h/16h\1h 150°C
	61	2	2	0.0	21.4	20.0	60.0	35.8	
	62	2	2	0.0	21.4	20.0	60.0	25.8	
	63	2	2	0.0	21.4	20.0	60.0	15.8	
	64	2	2	10.0	21.4	20.0	60.0	35.8	

	65	2	2	20.0	21.4	20.0	60.0	25.8	
	66	2	2	30.0	21.4	20.0	60.0	15.8	
	67	2	2	0.0	21.4	20.0	60.0	35.8	1h/6h\1h 180°C
	68	2	2	0.0	21.4	20.0	60.0	25.8	
	69	2	2	0.0	21.4	20.0	60.0	15.8	
	70	2	2	10.0	21.4	20.0	60.0	35.8	
	71	2	2	20.0	21.4	20.0	60.0	25.8	
	72	2	2	30.0	21.4	20.0	60.0	15.8	
				1M HNO_3 [µL]			V DMF [µL]	V EtOH [µL]	1h/16h\1h 150°C
	73	2	2	10.0	21.4	20.0	60.0	35.8	
	74	2	2	20.0	21.4	20.0	60.0	25.8	
	75	2	2	30.0	21.4	20.0	60.0	15.8	
							V H_2O [µL]	V EtOH [µL]	
	76	2	2	10.0	21.4	20.0	60.0	35.8	
	77	2	2	20.0	21.4	20.0	60.0	25.8	
	78	2	2	30.0	21.4	20.0	60.0	15.8	

Table S4. Molar ratios and exact amounts of the reactants employed in the HT experiments for MIL-53(Ga)-NH_2/NO_2.

metal source	No.	equivalent linker	equivalent In^{3+}	additive [µL/mg]	linker [mg]	In^{3+} [µL/mg]	V EtOH [µL]	V H_2O [µL]	temperature program
2M $In(NO_3)_3 \cdot H_2O$ in H_2O	1	1	0.5	0	10.0	11.1	10.0	128.9	1h/36h\1h 150°C
	2	1	1	0	10.0	22.1	10.0	117.9	
	3	1	2	0	10.0	44.2	10.0	95.8	
	4	2	1	0	20.0	22.1	10.0	117.9	
	5	2	2	0	20.0	44.2	10.0	95.8	
	6	2	4	0	20.0	88.5	10.0	51.5	
	7	1	0.5	0	10.0	11.1	20.0	118.9	
	8	1	1	0	10.0	22.1	20.0	107.9	
	9	1	2	0	10.0	44.2	20.0	85.8	
	10	2	1	0	20.0	22.1	20.0	107.9	
	11	2	2	0	20.0	44.2	20.0	85.8	
	12	2	4	0	20.0	88.5	20.0	41.5	
	13	1	0.5	0	10.0	11.1	40.0	98.9	8h/16h\4h 150°C
	14	1	1	0	10.0	22.1	40.0	87.9	
	15	1	2	0	10.0	44.2	40.0	65.8	
	16	2	1	0	20.0	22.1	40.0	87.9	
	17	2	2	0	20.0	44.2	40.0	65.8	
	18	2	4	0	20.0	88.5	40.0	21.5	
	19	1	0.5	0	10.0	11.1	60.0	78.9	
	20	1	1	0	10.0	22.1	60.0	67.9	

	21	1	2	0	10.0	44.2	60.0	45.8	
	22	2	1	0	20.0	22.1	60.0	67.9	
	23	2	2	0	20.0	44.2	60.0	45.8	
	24	2	4	0	20.0	88.5	60.0	1.5	
	25	2	2	0	20.0	44.2	10.0	95.8	24h/24h\12h 150°C
	26	2	2	0	20.0	44.2	20.0	85.8	
	27	2	2	0	20.0	44.2	50.0	55.8	
	28	2	2	0	20.0	44.2	60.0	45.8	
	29	2	2	0	20.0	44.2	85.0	20.8	
	30	2	2	0	20.0	44.2	100.0	5.8	
	31	2	2	0	20.0	44.2	10.0	95.8	4h/16h\8h 150°C
	32	2	2	0	20.0	44.2	20.0	85.8	
	33	2	2	0	20.0	44.2	50.0	55.8	
	34	2	2	0	20.0	44.2	60.0	45.8	
	35	2	2	0	20.0	44.2	85.0	20.8	
	36	2	2	0	20.0	44.2	100.0	5.8	
	37	2	2	0	20.0	44.2	10.0	95.8	12h/36h\12h 130°C
	38	2	2	0	20.0	44.2	60.0	45.8	
	39	2	2	0	20.0	44.2	100.0	5.8	
	40	2	1	0	20.0	22.1	20.0	107.9	
	41	2	2	0	20.0	44.2	20.0	85.8	
	42	2	4	0	20.0	88.5	20.0	41.5	
	43	2	2	0	20.0	44.2	30.0	225.8	
	44	2	2	0	20.0	44.2	150.0	105.8	
	45	2	2	0	20.0	44.2	250.0	5.8	
	46	2	1	0	20.0	22.1	50.0	227.9	
	47	2	2	0	20.0	44.2	50.0	205.8	
	48	2	4	0	20.0	88.5	50.0	161.5	
								V DMF [µL]	
	49	2	2	0	20.0	44.2	10.0	95.8	
	50	2	2	0	20.0	44.2	60.0	45.8	
	51	2	2	0	20.0	44.2	100.0	5.8	
	52	2	1	0	20.0	22.1	20.0	107.9	
	53	2	2	0	20.0	44.2	20.0	85.8	
	54	2	4	0	20.0	88.5	20.0	41.5	
	55	2	2	0	20.0	44.2	30.0	225.8	
	56	2	2	0	20.0	44.2	150.0	105.8	
	57	2	2	0	20.0	44.2	250.0	5.8	
	58	2	1	0	20.0	22.1	50.0	227.9	
	59	2	2	0	20.0	44.2	50.0	205.8	
	60	2	4	0	20.0	88.5	50.0	161.5	
				2M NaOH [µL]			V H_2O [µL]		1h/16h\1 h 150°C
	61	2	2	0.0	21.4	20.0	60.0	35.8	

	62	2	2	0.0	21.4	20.0	60.0	25.8	
	63	2	2	0.0	21.4	20.0	60.0	15.8	
	64	2	2	10.0	21.4	20.0	60.0	35.8	
	65	2	2	20.0	21.4	20.0	60.0	25.8	
	66	2	2	30.0	21.4	20.0	60.0	15.8	
	67	2	2	0.0	21.4	20.0	60.0	35.8	1h/6h\1h 180°C
	68	2	2	0.0	21.4	20.0	60.0	25.8	
	69	2	2	0.0	21.4	20.0	60.0	15.8	
	70	2	2	10.0	21.4	20.0	60.0	35.8	
	71	2	2	20.0	21.4	20.0	60.0	25.8	
	72	2	2	30.0	21.4	20.0	60.0	15.8	
				1M HNO_3 [µL]			V DMF [µL]	V EtOH [µL]	1h/16h\1h 150°C
	73	2	2	10.0	21.4	20.0	60.0	35.8	
	74	2	2	20.0	21.4	20.0	60.0	25.8	
	75	2	2	30.0	21.4	20.0	60.0	15.8	
							V H_2O [µL]	V EtOH [µL]	
	76	2	2	10.0	21.4	20.0	60.0	35.8	
	77	2	2	20.0	21.4	20.0	60.0	25.8	
	78	2	2	30.0	21.4	20.0	60.0	15.8	
2M $In(NO_3)_3 \cdot H_2O$ in DMF							V EtOH [µL]	V DMF [µL]	12h/36h\12h 130°C
		2	2	0	20.0	44.2	10.0	95.8	
		2	2	0	20.0	44.2	60.0	45.8	
		2	2	0	20.0	44.2	100.0	5.8	
		2	1	0	20.0	22.1	20.0	107.9	
		2	2	0	20.0	44.2	20.0	85.8	
		2	4	0	20.0	88.5	20.0	41.5	
		2	2	0	20.0	44.2	30.0	225.8	
		2	2	0	20.0	44.2	150.0	105.8	
		2	2	0	20.0	44.2	250.0	5.8	
		2	1	0	20.0	22.1	50.0	227.9	
		2	2	0	20.0	44.2	50.0	205.8	
		2	4	0	20.0	88.5	50.0	161.5	
		1	0.5	0	10.0	11.1	10.0	128.9	1h/6h\1h 150°C
		1	1	0	10.0	22.1	10.0	117.9	
		1	2	0	10.0	44.2	10.0	95.8	
		2	1	0	20.0	22.1	10.0	117.9	
		2	2	0	20.0	44.2	10.0	95.8	
		2	4	0	20.0	88.5	10.0	51.5	
		1	0.5	0	10.0	11.1	20.0	118.9	
		1	1	0	10.0	22.1	20.0	107.9	
		1	2	0	10.0	44.2	20.0	85.8	

		2	1	0	20.0	22.1	20.0	107.9
		2	2	0	20.0	44.2	20.0	85.8
		2	4	0	20.0	88.5	20.0	41.5
		1	0.5	0	10.0	11.1	40.0	98.9
		1	1	0	10.0	22.1	40.0	87.9
		1	2	0	10.0	44.2	40.0	65.8
		2	1	0	20.0	22.1	40.0	87.9
		2	2	0	20.0	44.2	40.0	65.8
		2	4	0	20.0	88.5	40.0	21.5
		1	0.5	0	10.0	11.1	60.0	78.9
		1	1	0	10.0	22.1	60.0	67.9
		1	2	0	10.0	44.2	60.0	45.8
		2	1	0	20.0	22.1	60.0	67.9
		2	2	0	20.0	44.2	60.0	45.8
		2	4	0	20.0	88.5	60.0	1.5

XRD patterns and refinements

MIL-53(Al)-NH_2/NO_2 (1) synthesized in DMF

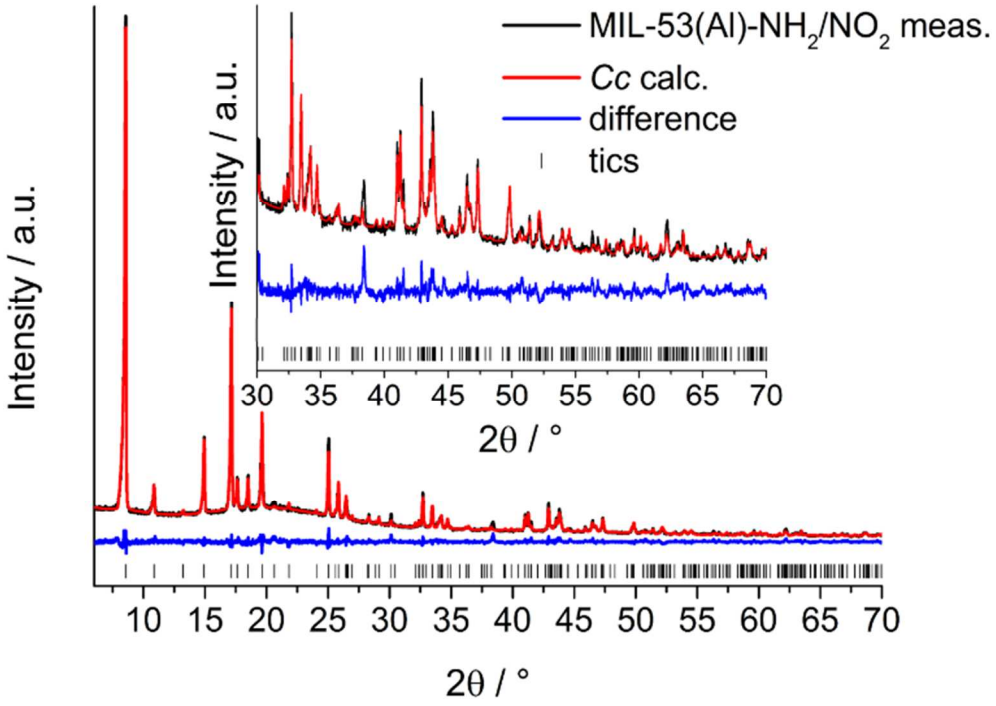

Figure S6. Final Rietveld plot of MIL-53(Al)-NH_2/NO_2 synthesized in DMF (**1**).

MIL-53(Al)-NH_2/NO_2 (2) synthesized in EtOH

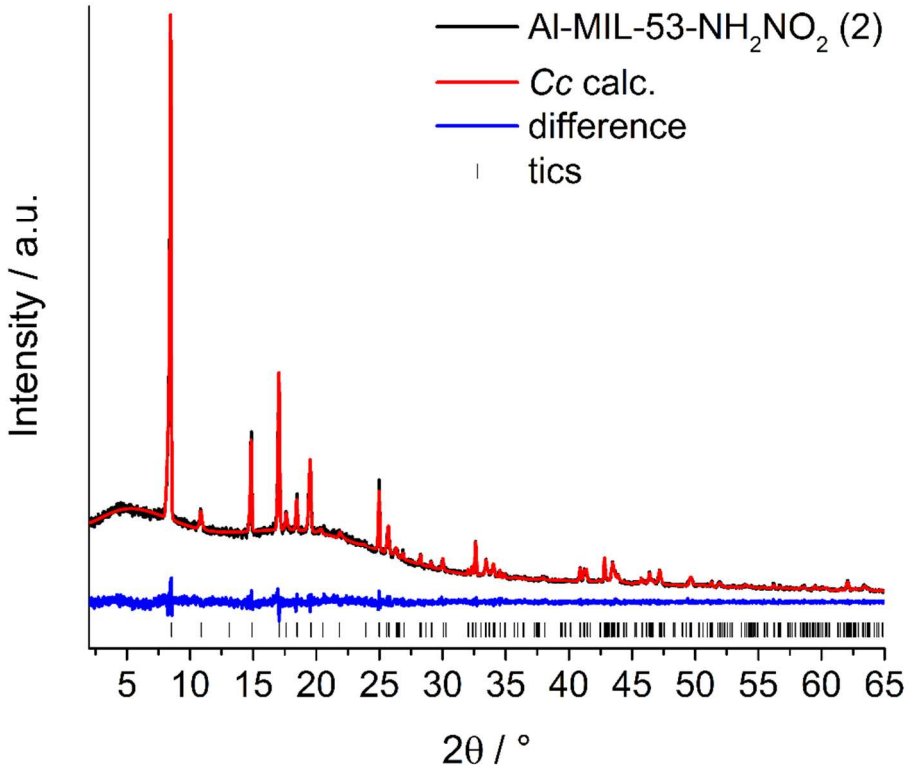

Figure S7. Pawley refinement of MIL-53(Al)-NH_2/NO_2 (**2**) synthesized in EtOH (**2**).

MIL-53(Ga)-NH_2/NO_2 (3)

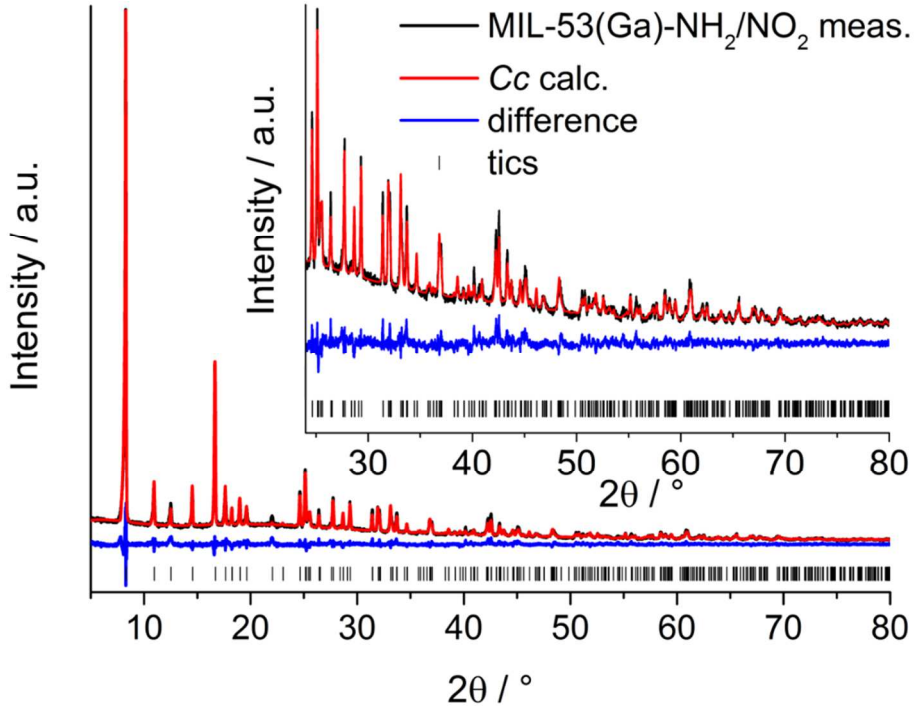

Figure S8. Final Rietveld plot of MIL-53(Ga)-NH_2/NO_2.(**3**).

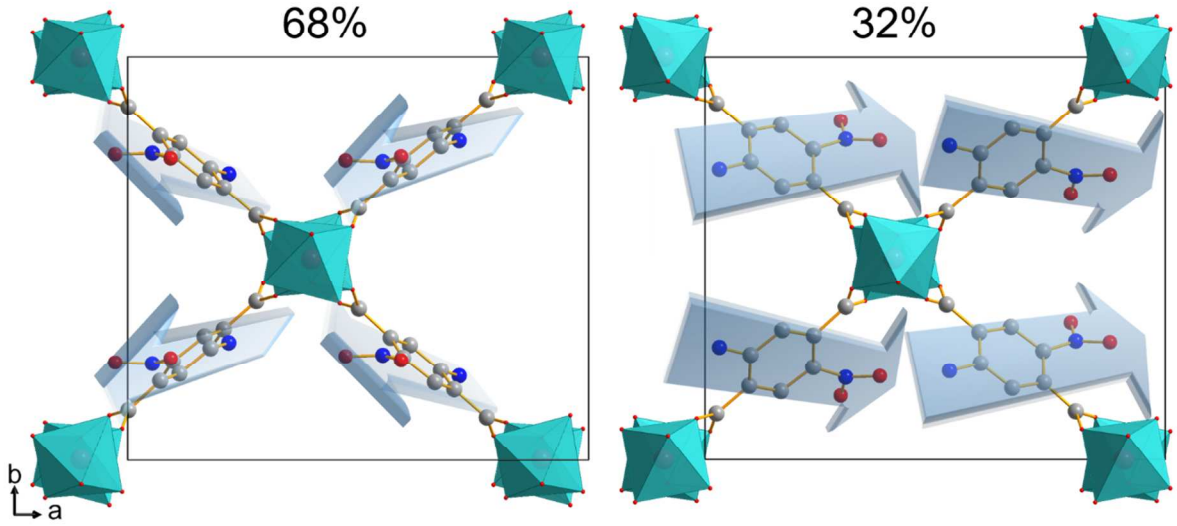

Figure S9. Crystal structure of MIL-53(Ga) along [001]. The disordering (above) of the structure contains 68% of the NO_2 groups of the linker molecules showing out of the plane and 39% pointing in plane. Carbon atoms are shown in grey, oxygen in red, nitrogen in blue and GaO_6 polyhedra in turquoise.

MIL-53(In)-NH_2/NO_2 (4)

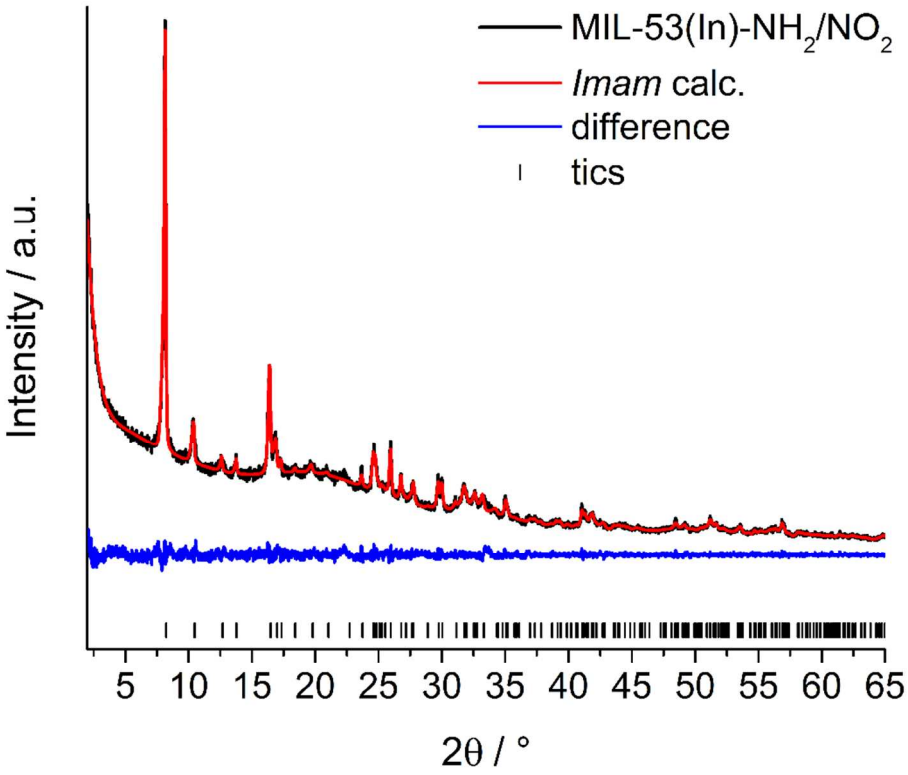

Figure S10. Plot of the Pawley refinement of MIL-53(In)-NH_2/NO_2 (**4**).

MIL-53(Al)-NH_2/NO_2 vnp (5), the XRD pattern of the as synthesized material is shown in the manuscript

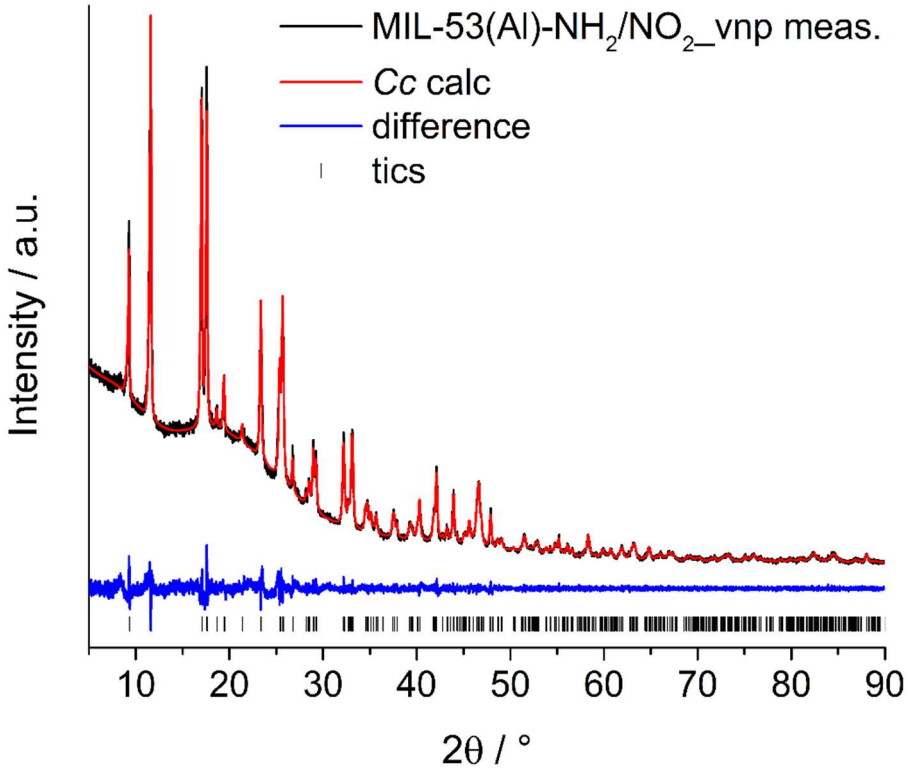

Figure S11. Pawley refinement of MIL-53(Al)-NH_2/NO_2_vnp (**5**).

Table S5. Results of the Pawley refinement of MIL-53(Al)-NH_2/NO_2_vnp.

MIL-53(Al)-NH_2/NO_2_vnp	
a / Å	20.125(1)
b / Å	8.2940(6)
c / Å	6.6506(4)
β / °	109.531(5)
space group	*Cc*
R_{wp} / %	3.04
GoF	1.86

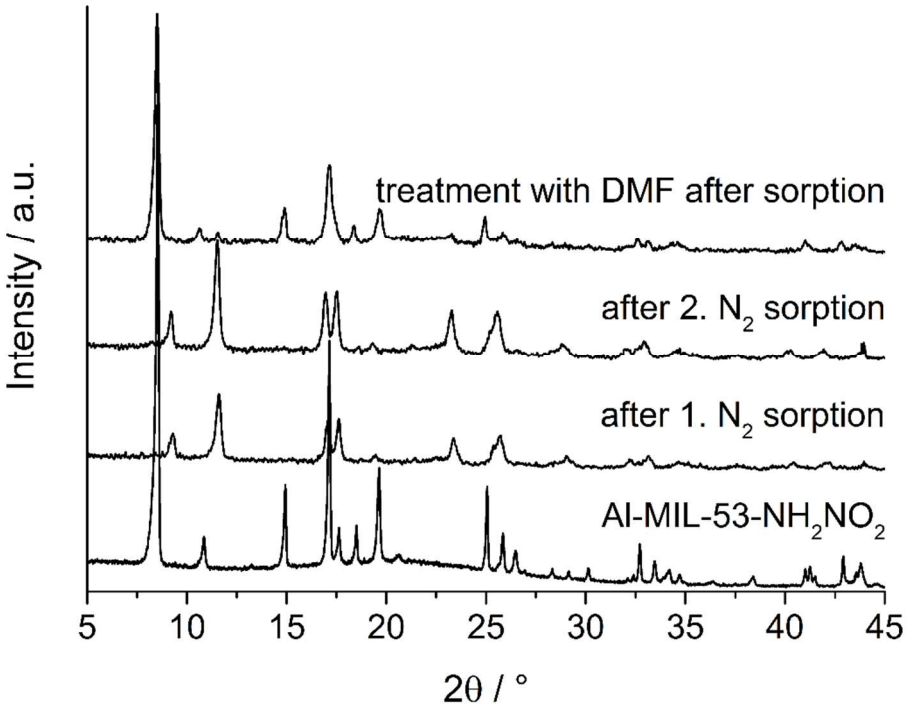

Figure S12. The vnp form of MIL-53(Al)-NH_2/NO_2 (**5**) obtained after N_2 sorption experiments (PXRDs shown in the middle) can be transformed to the as synthesized form (**1**, bottom) by immersion with DMF (top).

TG curves and elementary analysis

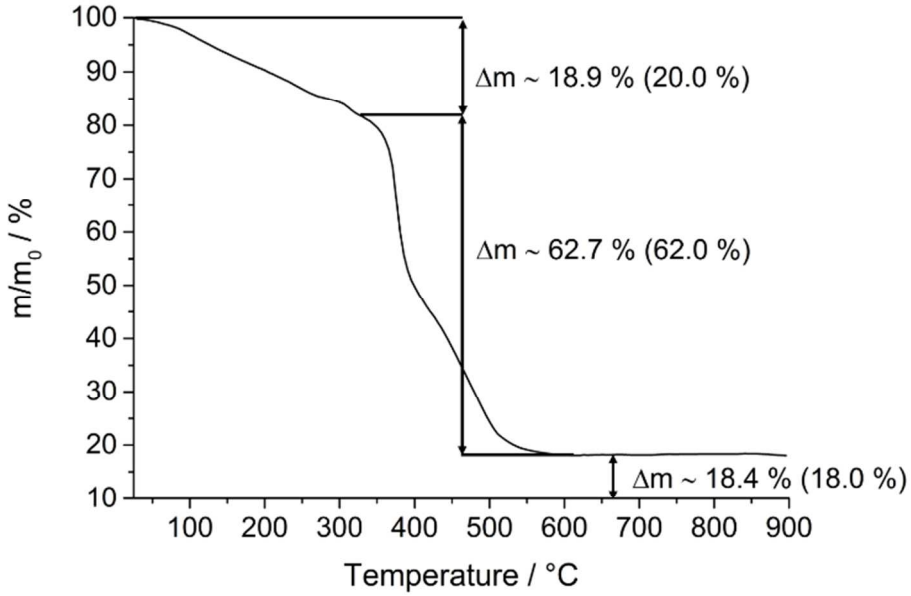

Figure S13. Thermogravimetric measurement for MIL-53(Al)-NH_2/NO_2 synthesized in DMF (**1**). Calculated values for the assumed sum formula are given in brackets.

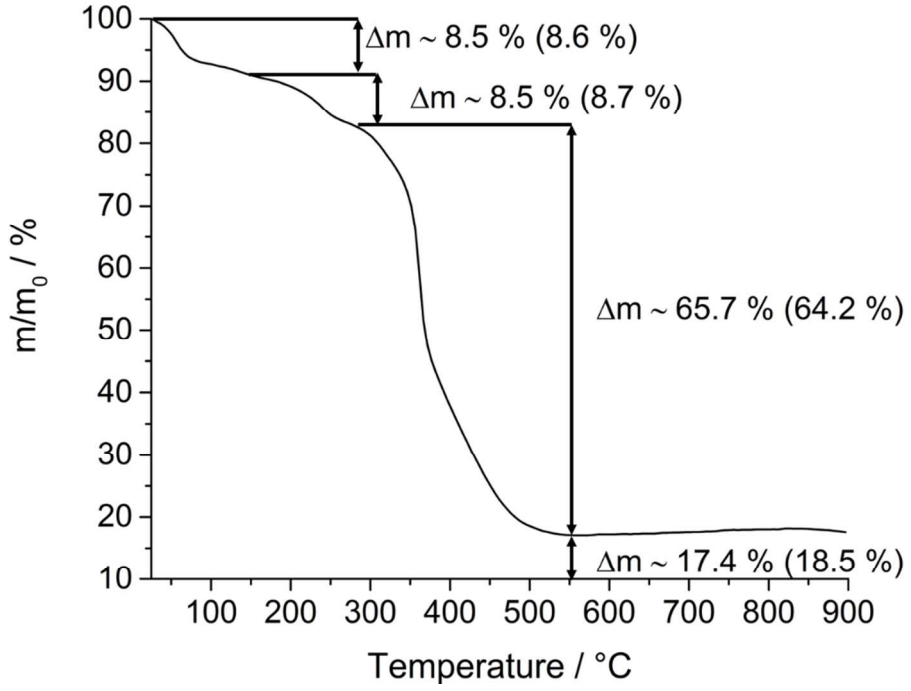

Figure S14. Thermogravimetric measurement for MIL-53(Al)-NH_2/NO_2 synthesized in EtOH (**2**). Calculated values for the assumed sum formula are given in brackets.

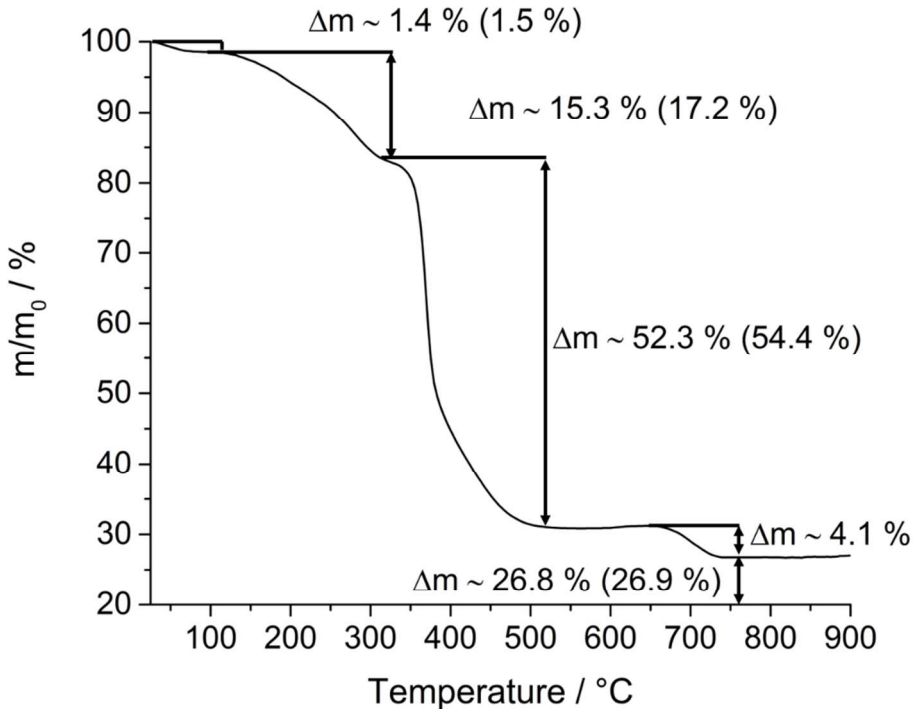

Figure S15. Thermogravimetric measurement for MIL-53(Ga)-NH_2/NO_2 (**3**). Calculated values for the assumed sum formula are given in brackets. The step at 700 °C is originating from the decomposition of Ga species like $Ga(NO_3)O$, $Ga(OH)_3$ and Ga(OH)O to Ga_2O_3.[1]

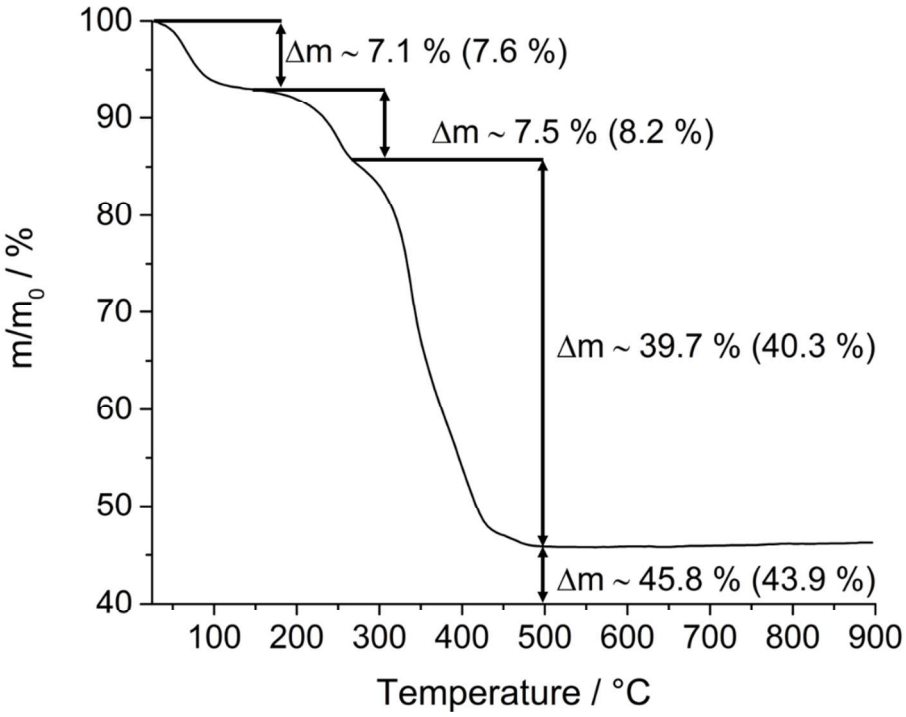

Figure S16. Thermogravimetric measurement for MIL-53(In)-NH_2/NO_2 (**4**). Calculated values for the assumed sum formula are given in brackets.

Table S6. Elementary analysis for the MIL-53 compounds. Sum formulas were obtained from thermogravimetric measurements.

compound		**C / %**	**H / %**	**N / %**
MIL-53(Al)-NH_2NO_2	calc.	38.5	3.4	12.2
[Al(OH)(BDC-NH_2NO_2)]·0.92DMF	meas.	38.0	3.2	11.8
MIL-53(Al)-NH_2NO_2 (2)	calc.	34.1	3.6	8.6
[Al(OH)(BDC-NH_2NO_2)]·0.61EtOH·1.57H_2O	meas.	37.1	2.8	9.2
MIL-53(Ga)-NH_2NO_2	calc.	34.4	3.2	10.6
[Ga(OH)(BDC-NH_2NO_2)]·0.13EtOH·1.9DMF	meas.	33.3	2.9	10.1
MIL-53(In)-NH_2NO_2	calc.	26.7	2.4	7.0
[In(OH)(BDC-NH_2NO_2)]·0.86EtOH·0.58DMF·0.43In_2O_3	meas.	23.4	2.0	5.9

SEM images

MIL-53(Al)-NH_2/NO_2 (1) synthesis in DMF

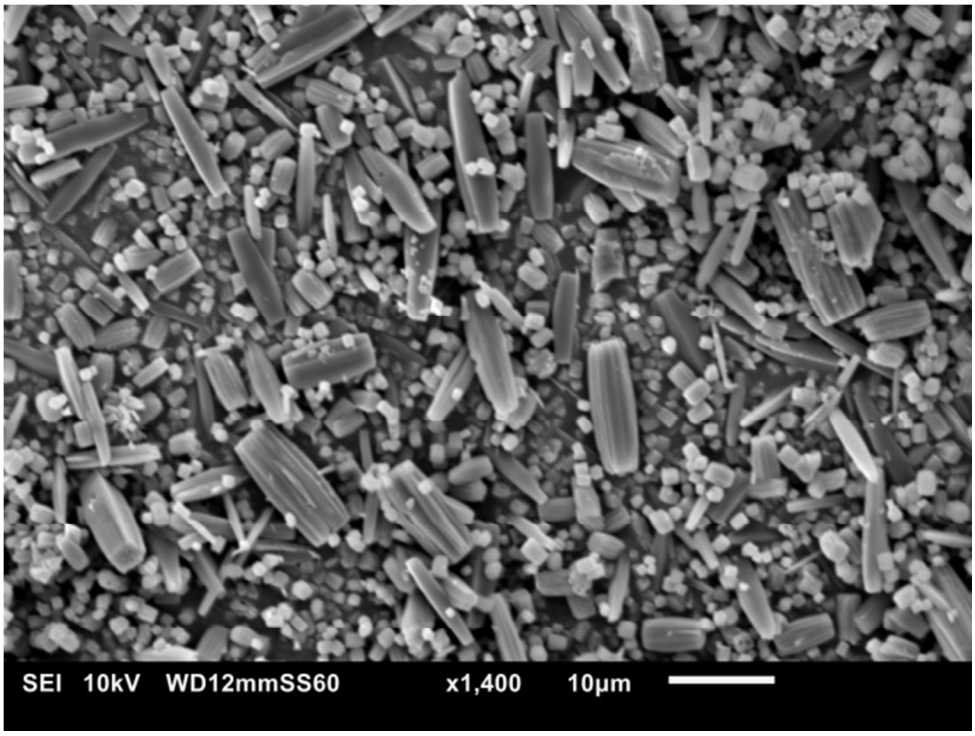

Figure S17. For MIL-53(Al)-NH_2/NO_2 (**1**) elongated more or less rectangular crystals with a size around 10 µm were obtained, along with small cubic crystals between 0.5-2 µm in size.

MIL-53(Al)-NH_2/NO_2 (2) synthesis in ethanol

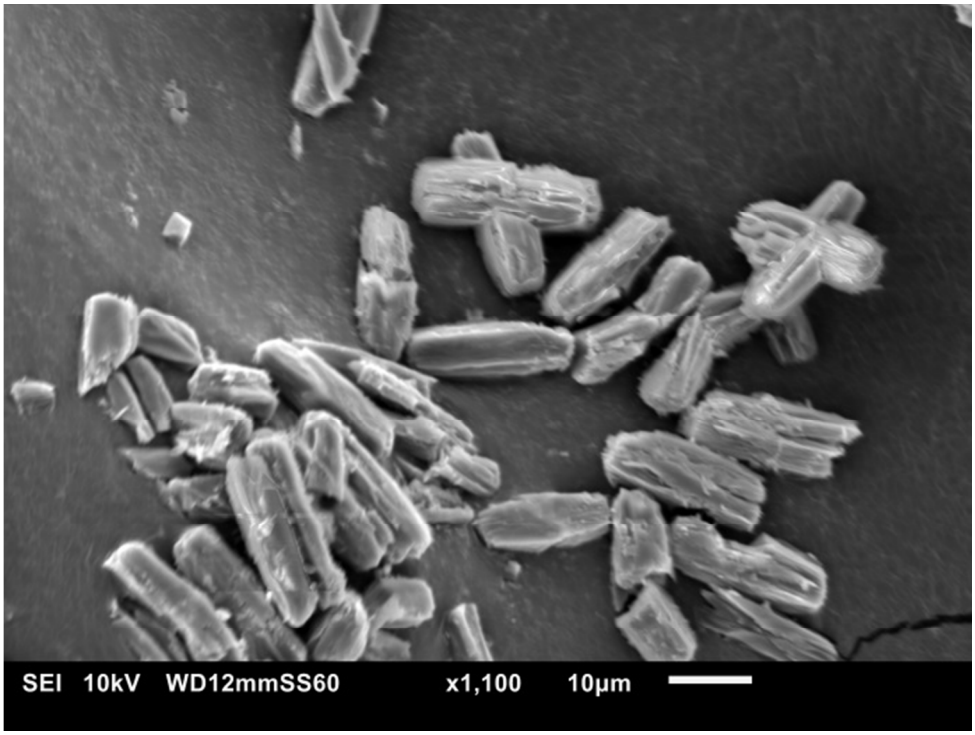

Figure S18. For MIL-53(Al)-NH_2/NO_2 (**2**) synthesized in ethanol, thicker crystals than for synthesis in DMF were obtained.

MIL-53(Ga)-NH_2/NO_2 (3)

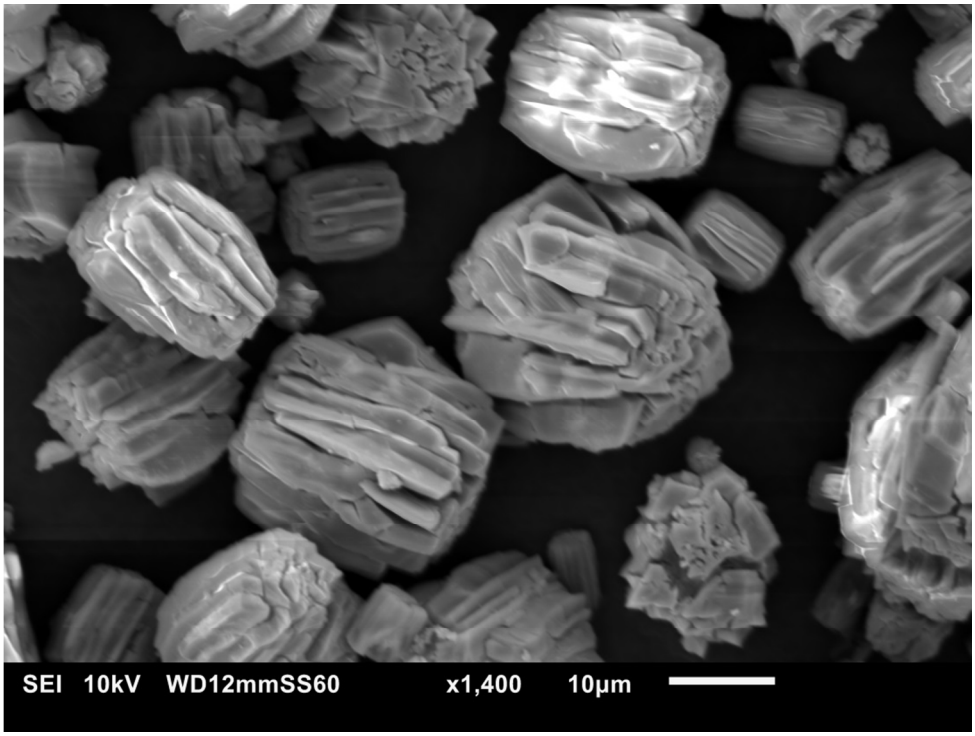

Figure S19. For MIL-53(Ga)-NH_2/NO_2 (**3**) aggregated crystals were obtained that seem to consist out of elongated rectangular crystals grown alongside each other.

MIL-53(In)-NH_2/NO_2 (4)

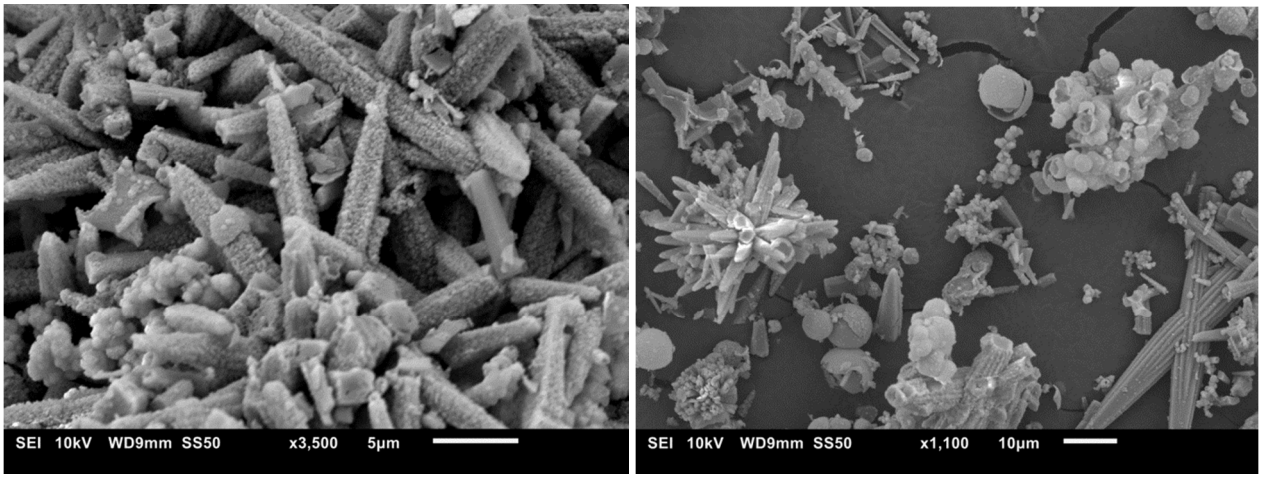

Figure S20. For MIL-53(In)-NH_2/NO_2 (**4**) only limited crystallinity was achieved, with crystals being very polycrystalline and aggregated.

NMR spectra

During the synthesis of MIL-53(Al)-NH_2/NO_2 (**2**) in ethanol, 15% of the amino groups were ethylated. **Figure S21** shows the numbering scheme of the linker molecule for the discussion in the NMR spectra. The allocation of the signals was confirmed by 2D NMR spectroscopy.

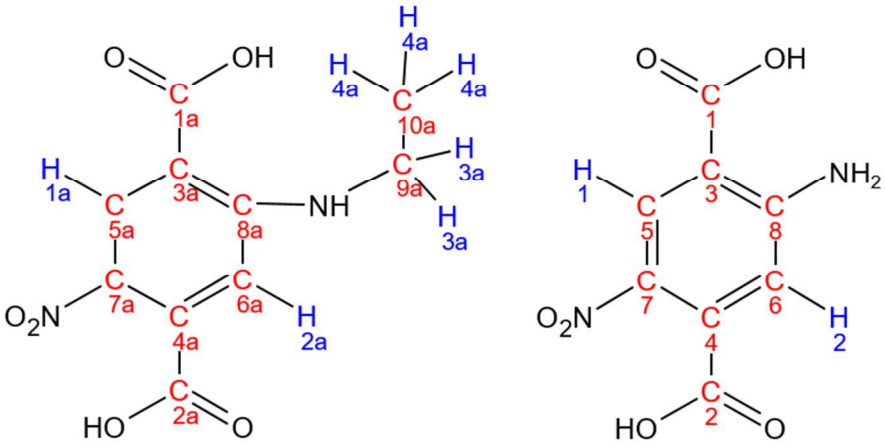

Figure S21. Numbering scheme of H_2BDC-NH_2/NO_2 (right) and the ethylated linker molecule (left) as it is used in the NMR spectra displayed.

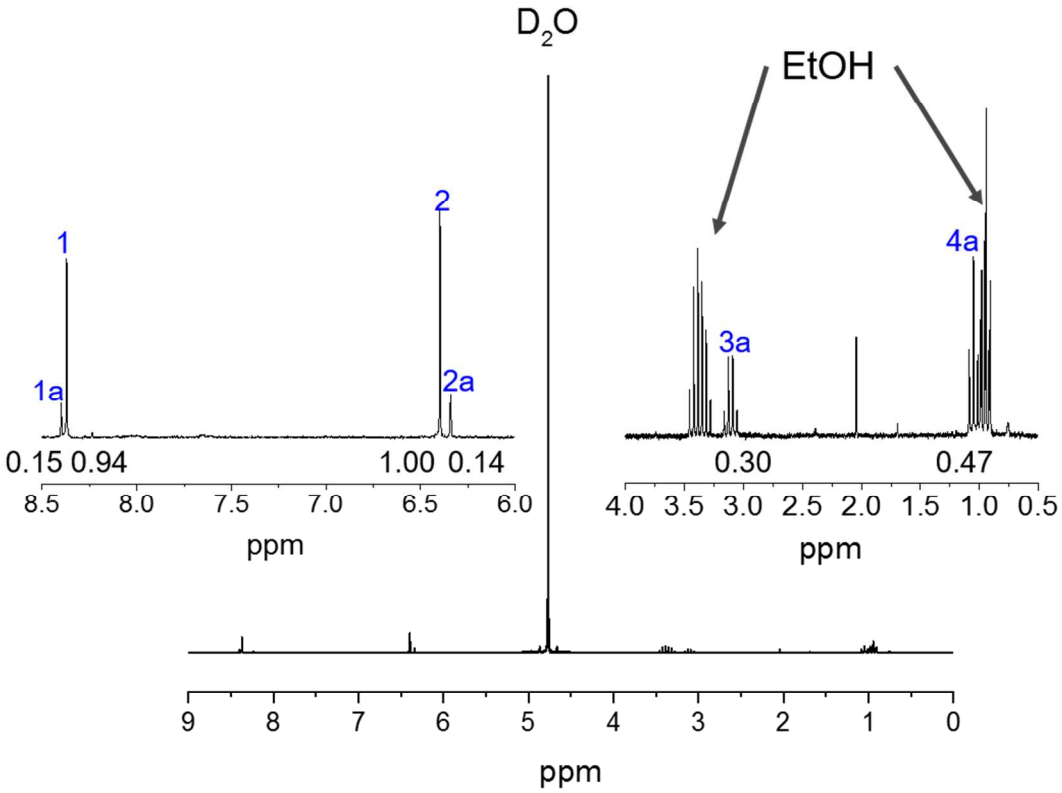

Figure S22. ^{1}H-NMR spectrum of MIL-53(Al)-NH_2/NO_2 (**2**) dissolved in 5% NaOD in D_2O. The integrals are displayed beneath the corresponding signals.

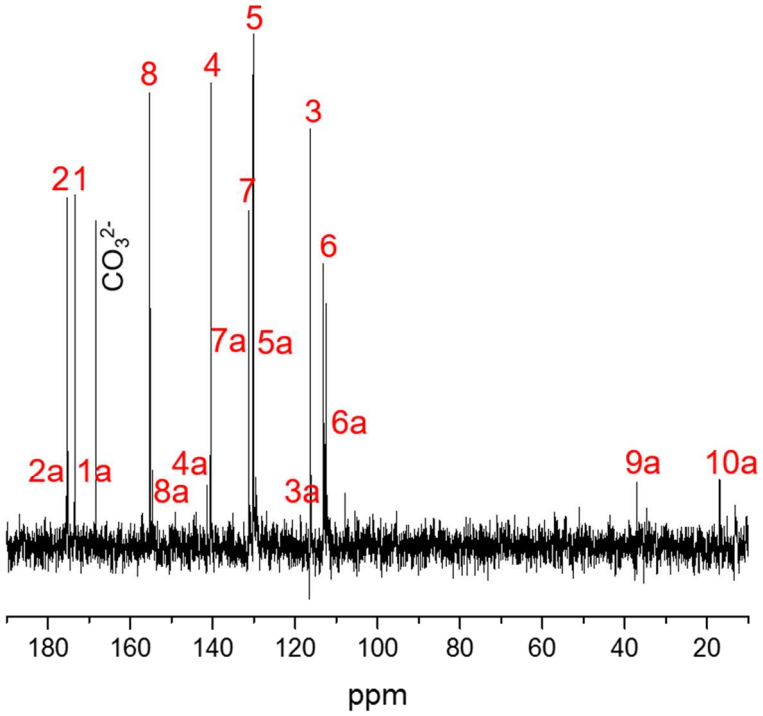

Figure S23. ^{13}C-NMR spectrum of MIL-53(Al)-NH_2/NO_2 (**2**) dissolved in 5% NaOD in D_2O. The carbonate peak is due to the solution of CO_2 in the solvent used.

Sorption experiments

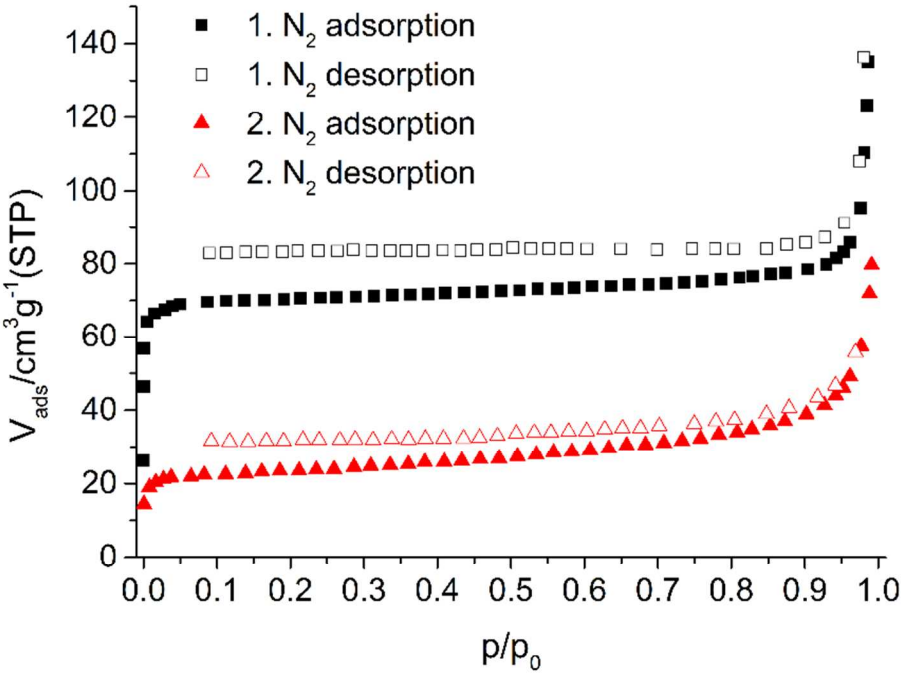

Figure S24. N_2 sorption isotherms of MIL-53(Al)-NH_2/NO_2 synthesized in DMF (**1**).

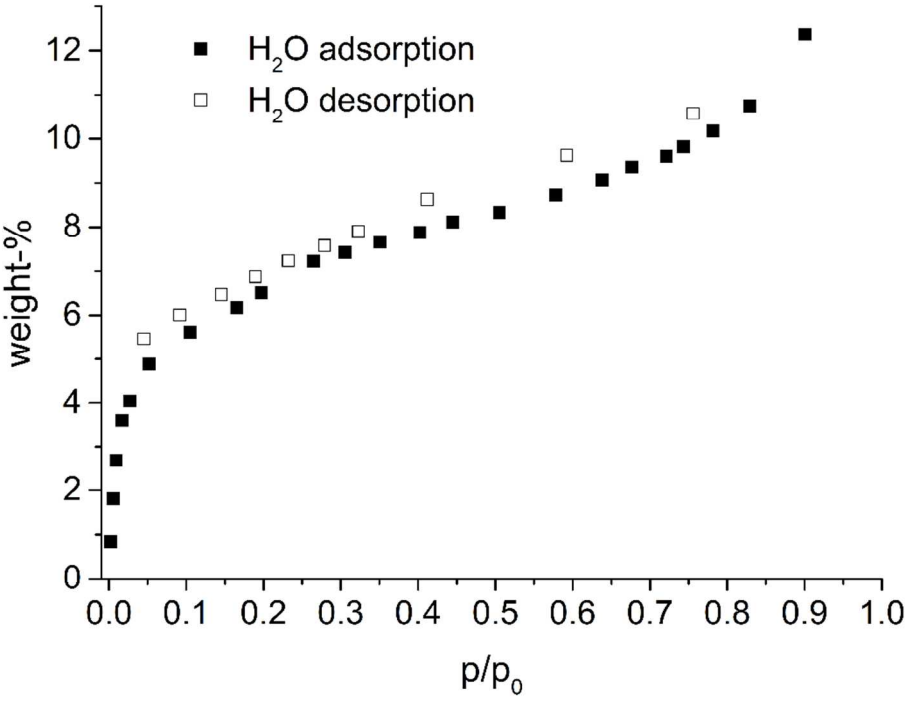

Figure S25. H_2O sorption isotherms of MIL-53(Al)-NH_2/NO_2 (**1**).

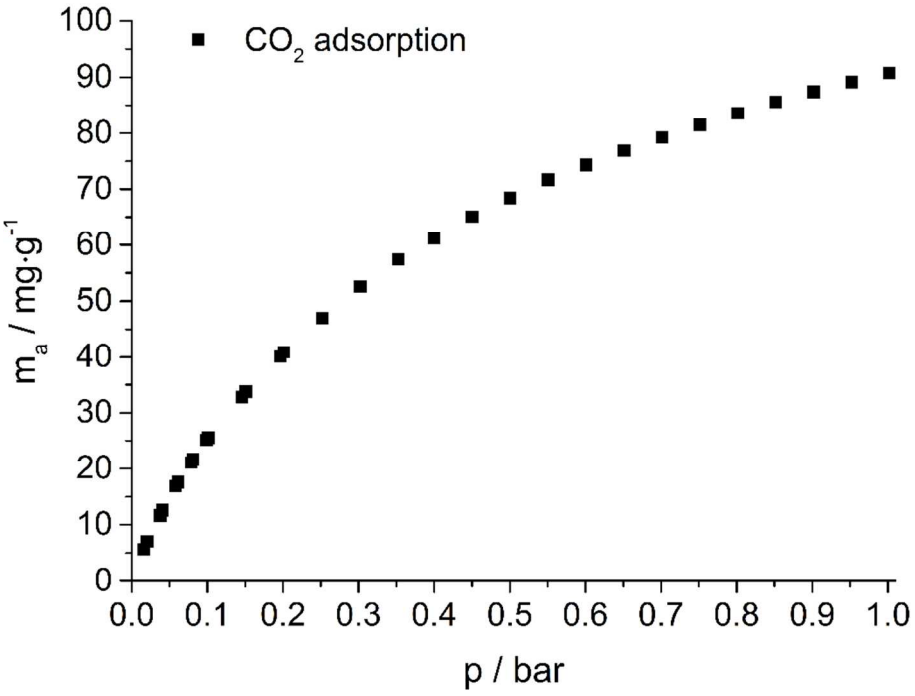

Figure S26. CO_2 sorption isotherm of MIL-53(Al)-NH_2/NO_2 (**1**).

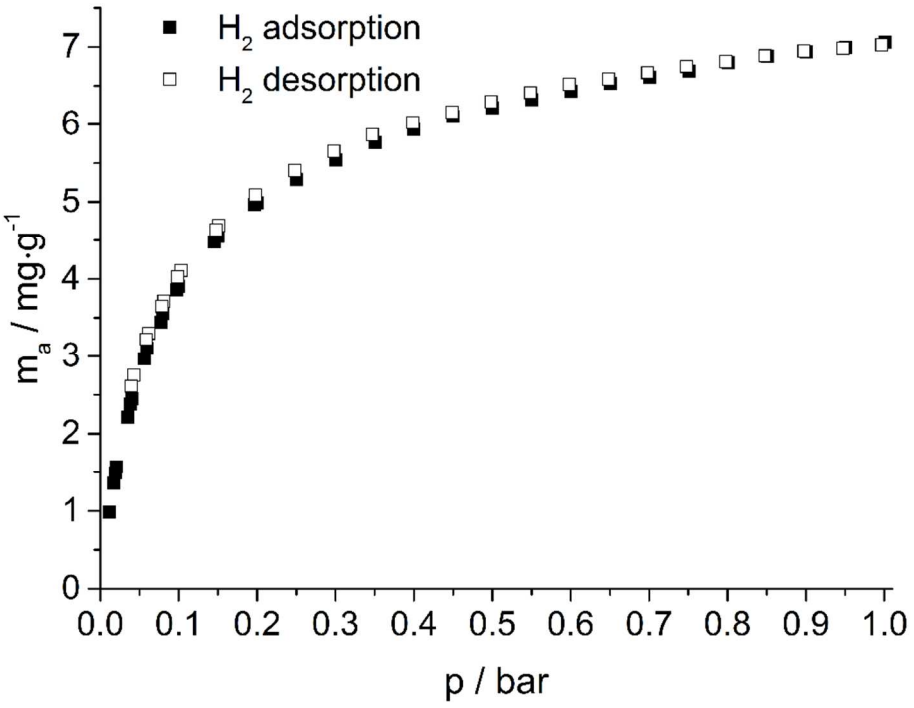

Figure S27. H_2 sorption isotherms of MIL-53(Al)-NH_2/NO_2 (**1**).

SHG microscopy

MIL-53(Al)-NH_2/NO_2 (1) as synthesized in DMF

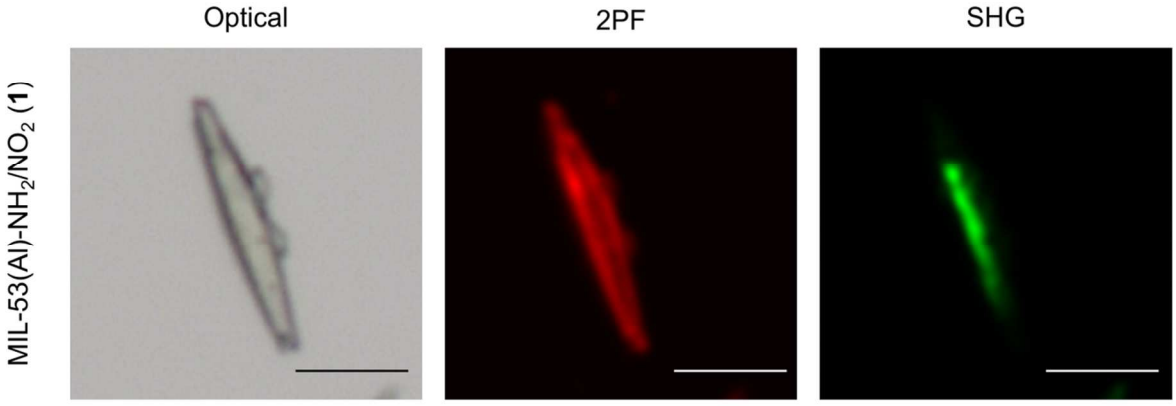

Figure S28. From left to right: optical, two-photon fluorescence and second harmonic generation images of MIL-53(Al)-NH_2/NO_2 (**1**). The SHG image displays the average intensity calculated over 60 images, each image being 3° apart in polarization direction of the incident polarized laser beam. The scale bars indicate a distance of 10 μm for each image.

MIL-53(Al)-NH_2/NO_2 (2) as synthesized in ethanol

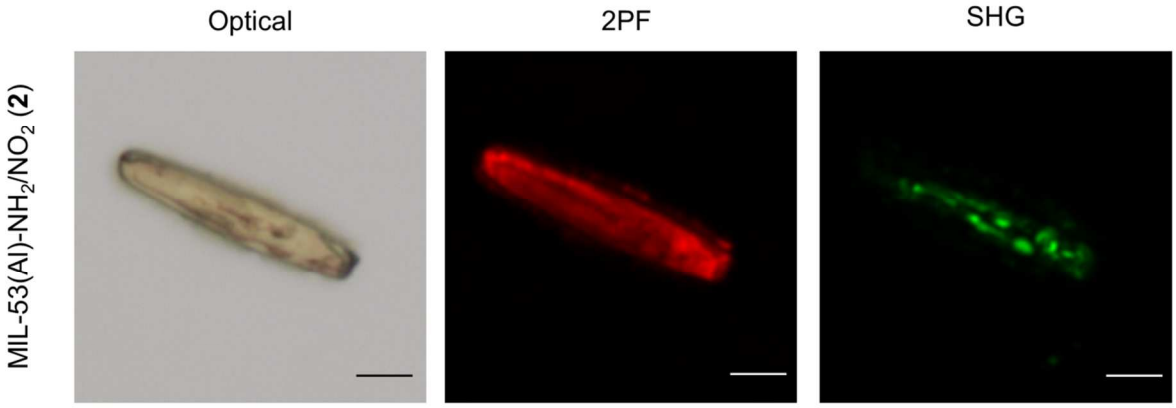

Figure S29. From left to right: optical, two-photon fluorescence and second harmonic generation images of MIL-53(Al)-NH_2/NO_2 (**2**). The SHG image displays the average intensity calculated over 60 images, each image being 3° apart in polarization direction of the incident polarized laser beam. The scale bars indicate a distance of 10 μm for each image.

MIL-53(In)-NH_2/NO_2 (4) as synthesized in DMF

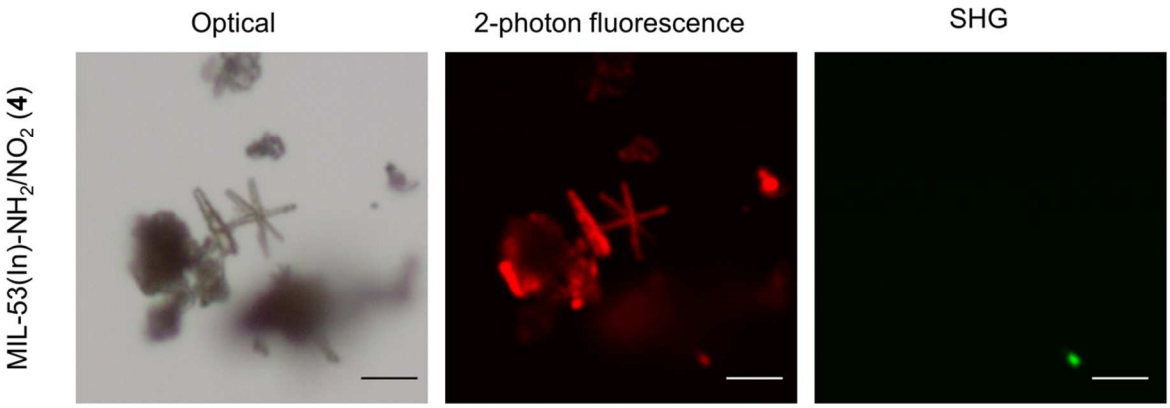

Figure S30. From left to right: optical, two-photon fluorescence and second harmonic generation images of MIL-53(In)-NH_2/NO_2 (**4**). The SHG image displays the average intensity calculated over 60 images, each image being 3° apart in polarization direction of the incident polarized laser beam. The scale bars indicate a distance of 10 μm for each image.

Calculation of <d_{eff}> values

To obtain the value for d_{eff}, the procedure as previously used by van der Veen *et al.* was followed.[2,3] Firstly, the SHG intensity of the sample was measured $(I_{2\omega,x})$ in an SHG wide field microscopy setup; next the SHG intensity of a reference sample was measured $(I_{2\omega,BBO})$. Beta barium borate (BBO) was used as a reference, 100 µm thick, cut to achieve type I phase matching and to optimize the quadratic nonlinear response (θ = 29.2°, φ = 90°; Eksma optics, BBO-601H). The formula for the second-order nonlinear coefficient <d_{eff}> was derived as follows:

$$I_{2\omega,x} = A\frac{< d_{\text{eff}} >^2 r^2 I_{\omega,x}^2}{n_{2\omega,x} n_{\omega,x}^2}$$

$$I_{2\omega,BBO} = A\frac{d_{ooe}^2 L^2 I_{\omega,BBO}^2}{n_{\theta,2\omega,BBO} n_{o,\omega,BBO}^2}$$

$$\Rightarrow \quad < d_{\text{eff}} > = \sqrt{\frac{I_{2\omega,x}}{I_{2\omega,BBO}} . d_{ooe}^2 . \frac{L^2}{r^2} . \frac{I_{\omega,BBO}^2}{I_{\omega,x}^2} . \frac{n_{2\omega,x} n_{\omega,x}^2}{n_{\theta,2\omega,BBO} n_{\theta,\omega,BBO}^2}}$$

With:

A = all the variables that are identical for both the sample and the BBO crystal

$I_{2\omega,x}$ = the SHG intensity of the sample

$I_{2\omega,BBO}$ = intensity of the SHG light of the BBO reference, measured with a plane of polarization of linearly polarized laser light for which the SHG intensity reaches a maximum

I_{ω} = the intensity of the incident laser light, linearly polarized

r = the height of the crystallites

$n_{2\omega}$ = the refractive index at the frequency of the second-harmonic light

n_{ω} = the refractive index at the frequency of the incident laser light

> The values of the refractive indices of metal-organic frameworks vary between 1.2 and 1.65 in the VIS to NIR spectral region.[4–6] We used a value of 1.5 for both $n_{2\omega}$ and n_{ω}, as this was the value determined for the related material MIL-53(Al)-NH_2.[2]

d_{ooe} = 2.01 pm/V = effective nonlinearity coefficient for type I phase-matched interaction for BBO

L = the thickness of the BBO crystal, 100 µm

$n_{\theta,2\omega,BBO}$ = extraordinary refractive index at the frequency of the SHG light, propagating at an angle θ with the optical axis of the crystal

$n_{o,\omega,BBO}^2$ = ordinary refractive index of BBO at the frequency of the incident light ω

Linearly polarized laser light was used to irradiate the sample and all the SHG signal was collected (no analyzer was positioned between the sample and the detector). To calculate the d_{eff} value for one crystal, the average over nine different orientations of linearly polarized laser light (all 10° apart) was calculated. To obtain the final <d_{eff}> value, the results were averaged over approximately 20 different crystals.

Ab initio calculations

Additional details about the multi-scale approach to calculate the macroscopic electric properties ($\chi^{(1)}$ and $\chi^{(2)}$ tensors). This method combines first principles calculations of the molecular properties with a classical electrostatic interactions scheme, known as the local field theory (LFT), to account for the crystal environment effects.[7–11] In LFT methodology, the $\chi^{(1)}$ and $\chi^{(2)}$ tensors read:

$$\underline{\underline{\chi}}^{(1)}(-\omega;\omega) = \frac{1}{\varepsilon_0 V}\sum_k \underline{\underline{d}}_k^T(\omega)\cdot\underline{\underline{\alpha}}_k(-\omega;\omega)$$

$$\underline{\underline{\underline{\chi}}}^{(2)}(-2\omega;\omega,\omega) = \frac{1}{2\varepsilon_0 V}\sum_k \underline{\underline{d}}_k^T(2\omega)\cdot\underline{\underline{\underline{\beta}}}_k(-2\omega;\omega,\omega):\underline{\underline{d}}_k^T(\omega)\underline{\underline{d}}_k^T(\omega)$$

where the k-sum runs over all (sub)molecules of the unit cell, α_k and β_k are the k-th (sub)molecule (hyper)polarizability tensors obtained by distributing evenly the ions (hyper)polarizabilities on the heavy atoms with the hydrogen atoms attached to them, ε_0 is the dielectric permittivity of vacuum, V is the unit cell volume and

$$\underline{\underline{d}}_k(\omega) = \sum_k \underline{\underline{D}}_{kk'}(\omega)$$

$$\underline{\underline{D}}^{-1}(\omega) = \left[\underline{\underline{1}} - \frac{1}{V\varepsilon_0}\underline{\underline{L}}\cdot\underline{\underline{\alpha}}(-\omega;\omega)\right]$$

where $\underline{\underline{L}}$ is the Lorentz factor tensor, $\underline{\underline{\alpha}}$ is the supermatrix of (sub)molecular polarizabilities. Therefore, $\underline{\underline{d}}_k$ interrelates the local electric field $\underline{F}_k$ (on the k-th (sub)molecule) with the macroscopic electric field $\underline{E}$:

$$\underline{F}_k = \underline{\underline{d}}_k\cdot\underline{E}$$

The $\chi^{(1)}$ tensor components were calculated in the abc* orthogonal reference frame and the $\chi^{(2)}$ tensor components are reported in the eigenbasis of the calculated dielectric tensor $\underline{\underline{\varepsilon}}(\omega) = \underline{\underline{1}} + \underline{\underline{\chi}}^{(1)}(\omega)$ whose eigenvectors are the squares of the refractive indices. The final $\chi^{(1)}$ and $\chi^{(2)}$ tensors of the investigated material (combining A and C phases) were obtained as weighted averages, first in the abc* frame, then the resulting $\chi^{(2)}$ was transformed to the optical indicatrix axes of the averaged $\underline{\underline{\varepsilon}}(\omega) = \underline{\underline{1}} + \underline{\underline{\chi}}^{(1)}(\omega)$ tensor (using the weights from the powder diffraction refinement).

The calculations of molecular properties, *α* and *β*, were performed for the individual cations (+2 charge) and anions (-2 charge) within their embedding electric field. Beforehand, starting from the X-ray diffraction data the geometry of the different crystals were optimized using periodic boundary conditions, the B3LYP exchange-correlation potential and the 6-31G(d,p) basis set. Only the fractional coordinates were optimized with the cell parameters kept fixed at their experimental values. The Crystal14 package[12] was employed. This in-crystal electric field was simulated by a 100 Å radius sphere of Mulliken point charges, calculated using the PBC/B3LYP/6-31G(d,p) method on the optimized crystal. The adequacy of this choice of charge definition has recently been discussed.[13] First, the static ($\lambda = \infty$) responses were evaluated at the second-order Møller-Plesset method (MP2) level. The dynamic MP2 (Møller-Plesset second-order perturbation theory) molecular properties were evaluated by employing a modified multiplicative scheme,[14] where the static MP2 values are combined with the static coupled-perturbed Kohn-Sham (CPKS) and dynamic time-dependent DFT (TDDFT) tensors evaluated using the B3LYP XC functional, following the scheme described in Ref. 15. At both levels, the selected basis set is the 6-

311++G(d,p) basis and it contains both diffuse and polarization functions for an accurate prediction of the linear and nonlinear molecular properties. All the molecular property calculations were performed with Gaussian09.[16] Performing calculations at the experimental incident wavelength of 800 nm was not possible since the *λ*/2 wavelength (400 nm) is already in the resonant regime of the anions, which leads to qualitatively wrong hyperpolarizability values. Additional TDDFT/B3LYP/6-311++G(d,p) calculations of the excitation energies of the anions in the crystal field confirmed that the first excitation energies correspond to a wavelength of 393 nm, 422 nm, and 325 nm for compounds **1**, **3**, and **4**, respectively, in close agreement with experiment. Nevertheless, the computational results at an incident wavelength of 1064 nm (SHG at 532 nm) are expected to be sufficiently close for analyzing the experimental results. Frequency/wavelength dependence of the macroscopic responses is further described in Tables S7-S8.

Using the $\chi^{(1)}$ and $\chi^{(2)}$ tensor components the d_{eff} values were calculated for types I and type II phase matchings (PM) conditions. The (non-polarized or polarized one when not aligned on the natural o or e polarization vectors, which is the general case) light beam traveling through anisotropic medium (biaxial crystal in our case) splits into two perpendicularly polarized beams [(+) and (-)] traveling at different speeds inversely proportional to the refractive indices associated to those polarizations: with n+ > n- (v+ < v-, where v is the phase velocity). The second-order process involves interaction between three beams: two at fundamental frequency (ω) and one at the double frequency (2ω). The effectiveness of the SHG interaction is governed by the extent of the (+) and (-) index surfaces overlap for the two frequencies. Two possibilities are usually considered: i) interaction of the fundamental rays having (+) polarization with the SHG beam at (-) polarization (type I PM) and ii) fundamental rays having opposite polarizations (+ and -) with SHG at (-) polarization (type II PM). Then, having defined the polarization directions of the light waves using the polar angles (θ, ϕ) (with $0 \le \theta \le \pi$ and $0 \le \phi \le 2\pi$) the d_{eff} values are evaluated using:

$$d_{eff} = \frac{1}{2}\underline{e_i}(2\omega) \cdot \underline{\underline{\chi}}^{(2)} : \underline{e_j}(\omega)\, \underline{e_k}(\omega) \times sinc\left(\frac{\Delta k\, r}{2}\right)$$

where $\underline{e_i}$, $\underline{e_j}$ and $\underline{e_k}$ are the light waves polarization vectors, r is the optical path length (symbolizing the grain size in the calculation) and

$$\Delta k = \frac{2\pi}{\lambda}\Delta n;\ \Delta n = 2n_{2\omega}^{1} - n_{\omega}^{2} - n_{\omega}^{3}$$

is the phase mismatch related to the difference of refractive indices. 1, 2, and 3 refer to the crystal axes. Finally, all possible orientations of the light wave polarization with respect to the crystal grains, defined by the polar angles (θ, ϕ), are taken into account to provide the average $\langle d_{eff} \rangle$ quantities.

Table S7. MP2/LFT results for MIL-53(Al)-NH_2/NO_2 and MIL-53(Al)-NH_2 (in the very narrow pore phase): refractive indices, selected $\chi^{(2)}$ tensor components (pm/V), and $\langle d_{eff} \rangle$ (pm/V) for different grain sizes at different wavelengths (nm). For MIL-53(Al)-NH_2/NO_2, results are listed for the pure A and C phases as well as for the A/C mixture (A:C = 61:39 as obtained from XRD analysis).

Compound and phase	λ	n_1	n_2	n_3	$\chi^{(2)}_{333}$	$\chi^{(2)}_{111}$	$\chi^{(2)}_{133}$	$\langle d_{eff} \rangle$ r =0 μm	$\langle d_{eff} \rangle$ r =3 μm	$\langle d_{eff} \rangle$ r =10 μm
MIL-53(Al)-NH_2/NO_2 Phase A	∞	1.539	1.416	1.721	51.2	-1.1	-7.7	1.950	0.208	0.061
	1064	1.553	1.427	1.762	133.9	-1.5	-16.3	3.409	0.583	0.215
	532	1.611	1.469	1.974						
MIL-53(Al)-NH_2/NO_2 Phase C	∞	1.539	1.416	1.722	-51.3	1.1	7.6	1.954	0.208	0.062
	1064	1.553	1.427	1.762	-134.2	1.5	16.2	3.394	0.576	0.212
	532	1.611	1.469	1.975						
MIL-53(Al)-NH_2/NO_2 A/C (61:39)	∞	1.539	1.416	1.721	11.2	-0.2	-1.7	0.426	0.045	0.013
	1064	1.553	1.427	1.762	29.3	-0.3	-3.6	0.751	0.131	0.048
	532	1.611	1.469	1.974						
MIL-53(Al)-NH_2 (vnp)	∞	1.759	1.445	1.912	3.9	-8.1	-5.6	1.264	0.111	0.033
	1064	1.780	1.454	1.949	6.2	-15.8	-6.6	2.130	0.440	0.178
	532	1.862	1.496	2.116						

Table S8. MP2/LFT results for MIL-53(Ga)-NH_2/NO_2: refractive indices, selected $\chi^{(2)}$ tensor components (pm/V), and $\langle d_{eff} \rangle$ (pm/V) for different grain sizes at different wavelengths (nm). The results are listed for the pure A and C phases as well as for the A/C mixture (A:C = 68:32 as obtained from XRD analysis).

Compound and phase	λ	n_1	n_2	n_3	$\chi^{(2)}_{333}$	$\chi^{(2)}_{111}$	$\chi^{(2)}_{133}$	$\chi^{(2)}_{113}$	$\langle d_{eff} \rangle$ r =0 μm	$\langle d_{eff} \rangle$ r =3 μm	$\langle d_{eff} \rangle$ r =10 μm
MIL-53(Ga)-NH_2/NO_2 Phase A	∞	1.708	1.380	1.480	-1.9	69.0	-2.2	4.5	1.752	0.171	0.053
	1064	1.757	1.389	1.494	-4.4	222.2	-6.9	13.3	2.952	0.541	0.209
	532	2.062	1.436	1.560							
MIL-53(Ga)-NH_2/NO_2 Phase C	∞	1.668	1.373	1.469	2.0	-47.7	2.1	-3.2	1.428	0.166	0.049
	1064	1.703	1.383	1.488	4.3	-147.1	7.0	-4.9	3.089	0.828	0.332
	532	1.922	1.436	1.582							
MIL-53(Ga)-NH_2/NO_2 A/C (68:32)	∞	1.695	1.378	1.477	-0.5	31.8	-1.0	1.0	0.715	0.076	0.023
	1064	1.740	1.387	1.493	-1.3	105.0	-3.2	1.9	1.221	0.272	0.107
	532	2.014	1.436	1.574							

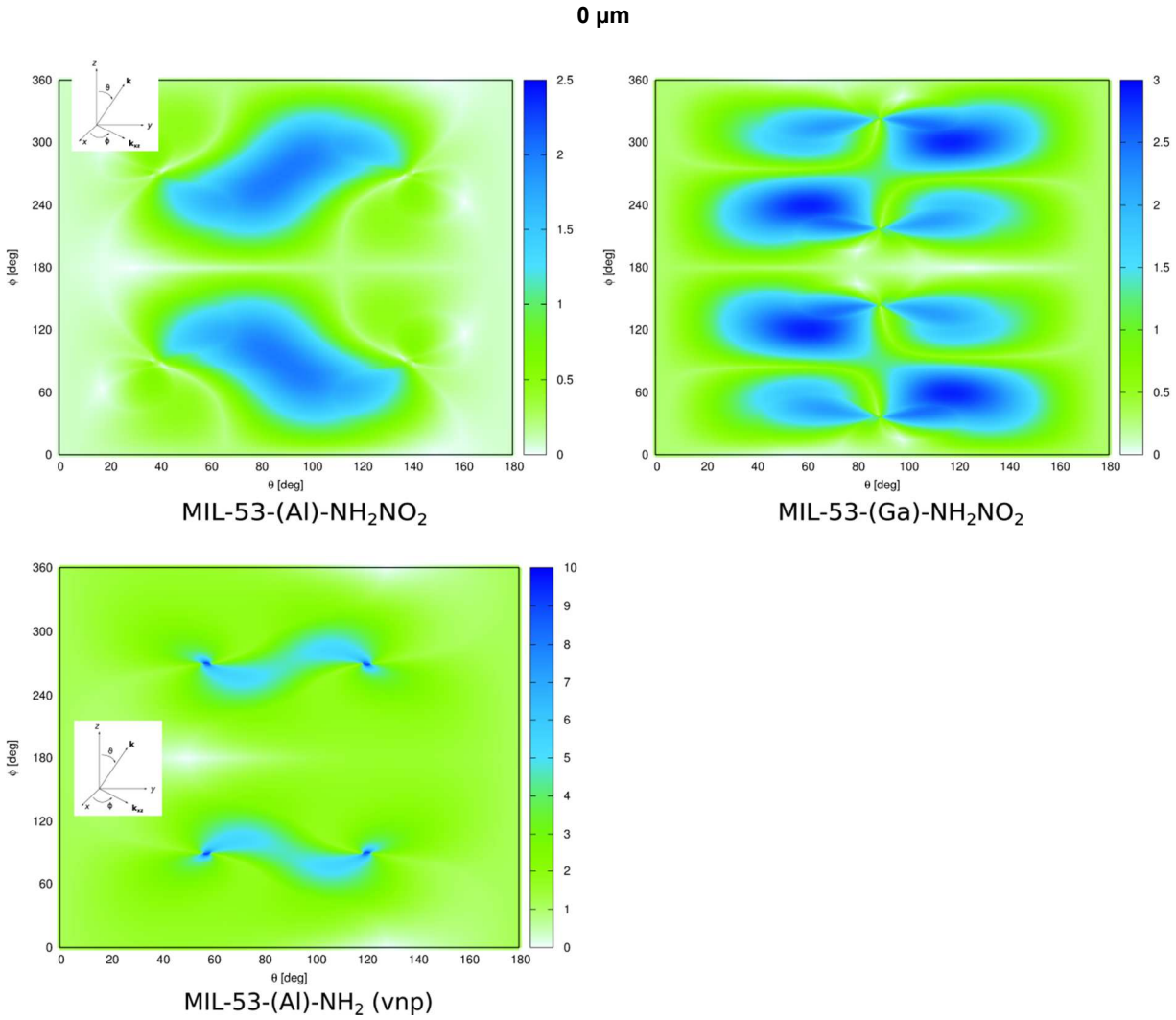

Figure S31. Angular dependence of the calculated d_{eff} (in pm/V) for MIL-53-(Al)-NH_2/NO_2, MIL-53(Ga)-NH_2/NO_2, and MIL-53(Al)-NH_2 (vnp) at λ =1064 nm for *r* = 0 µm (the inset gives the definition of the polar angles (θ,ϕ), k being the wave vector of light, corresponding to the direction of propagation).

3 µm

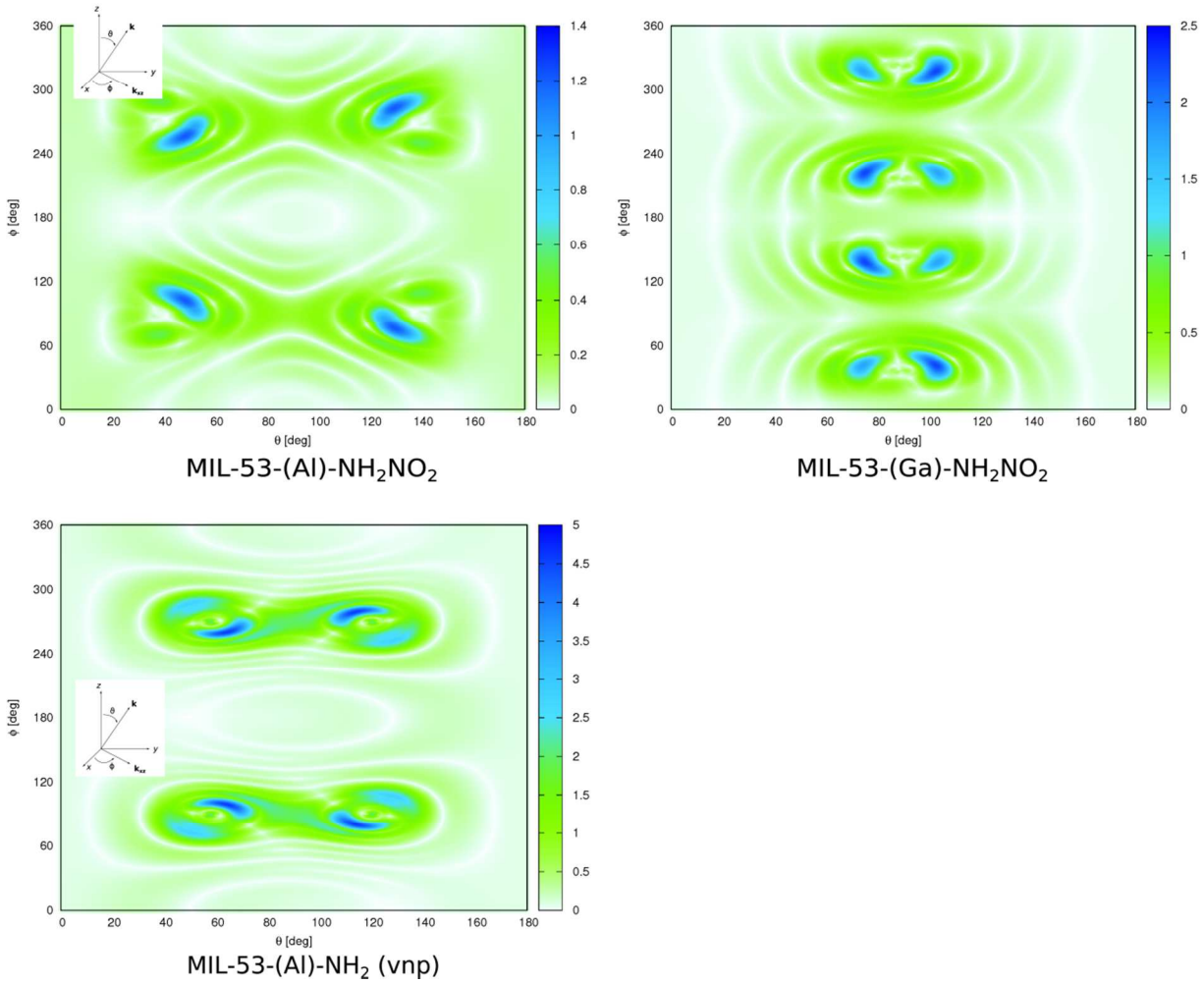

Figure S32. Angular dependence of the calculated d_{eff} (in pm/V) for MIL-53-(Al)-NH_2/NO_2, MIL-53(Ga)-NH_2/NO_2, and MIL-53(Al)-NH_2 (vnp) at λ =1064 nm for *r* = 3 µm (the inset gives the definition of the polar angles (θ,ϕ), k being the wave vector of light, corresponding to the direction of propagation).

10 µm

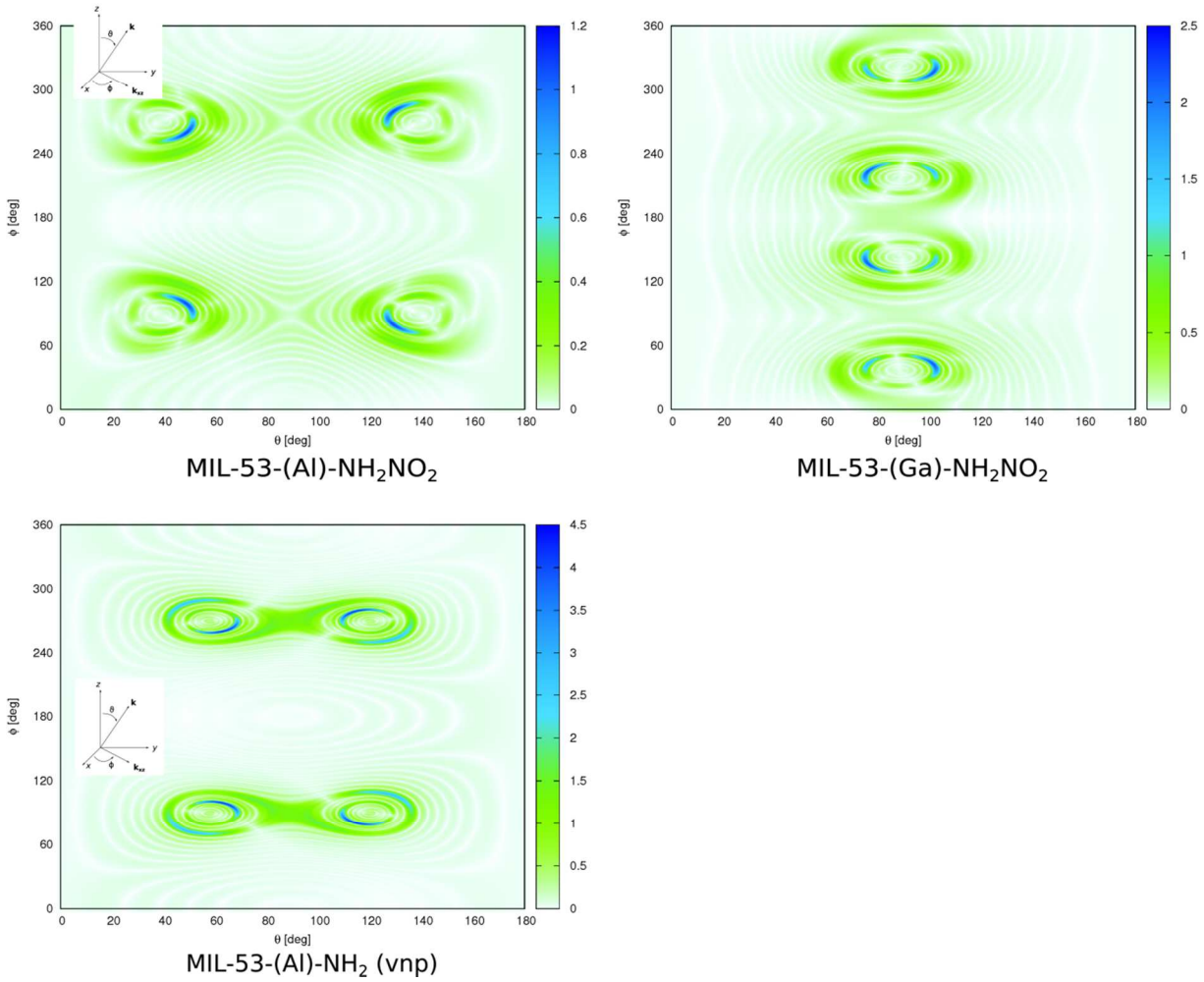

Figure S33. Angular dependence of the calculated d_{eff} (in pm/V) for MIL-53-(Al)-NH_2/NO_2, MIL-53(Ga)-NH_2/NO_2, and MIL-53(Al)-NH_2 (vnp) at λ =1064 nm for *r* = 10 µm (bottom) (the inset gives the definition of the polar angles (θ,ϕ), k being the wave vector of light, corresponding to the direction of propagation).

Estimation of the transmittance of 400 nm light through MIL-53(Al)-NH_2-NO_2 crystals

To estimate the transmittance of the generated 400 nm SHG light through the MIL-53(Al)-NH_2-NO_2 crystals we can use the law of Lambert Beer:

$$A = \varepsilon lc = log\frac{I_0}{I} = \log\frac{1}{T} \quad [1]$$

With: A the absorbance

T the transmittance

ε the molar extinction coefficient

l the path length of the beam of light through the material sample

c the amount concentration of the attenuating species in the material sample

I_0 the incident intensity

I the transmitted intensity

To calculate the transmittance T, we can convert formula [1] to:

$$T = 10^{-\varepsilon lc} \quad [2]$$

For MIL-53(Al)-NH_2-NO_2 crystals, the transmittance T can be estimated using the following values:

- For the molar extinction coefficient, we use the molar extinction coefficient of PNA: $\varepsilon_{400\,nm}(PNA) = 12300\ \frac{L}{mol.cm}$ determined by Bru et al. for free PNA in water[17]
- The average path length of generated 400 nm SHG light in MIL-53(Al)-NH_2-NO_2 crystals with an average height of 2 µm is: $l = 1\ \mu m$
- The concentration relates to the number density through the following equation:

$$c = \frac{n}{\mathrm{N_A}} \quad [3]$$

With: n the number density of the attenuating species in the material sample

$\mathrm{N_A}$ the Avogadro constant = 6.022 x 10^{23} mol^{-1}

- The number density of the linker with PNA motif in MIL-53(Al)-NH_2-NO_2 can be derived from the crystal structure: $n = \frac{4}{1438.18}\frac{molecules}{Å^3}$

With these values we can estimate the transmittance of generated 400 nm SHG light trough MIL-53(Al)-NH_2-NO_2 crystals with a thickness of 2 µm to be 2.1 10^{-4} %:

$T = 10^{-\varepsilon lc}$

$$T = 10^{-[12300 \frac{L}{mol\ cm} \cdot 1\ \mu m \cdot \frac{4}{1438{,}18} \frac{molecules}{Å^3} \cdot \frac{1}{6{,}022\ .10^{23}} \frac{mol}{molecules}]}$$

$$T = 10^{-[12300 \frac{L}{mol\ cm} \cdot \frac{1 dm^3}{1\ \ L} \cdot 1\ \mu m \cdot \frac{10^{-4} cm}{1\ \ \mu m} \cdot \frac{4}{1438{,}18} \frac{molecules}{Å^3} \frac{1\ \ Å^3}{10^{-27} dm^3} \cdot \frac{1}{6{,}022\ .10^{23}} \frac{mol}{molecules}]}$$

$$T = 2{,}1.\ 10^{-6}$$

UV-vis spectrum

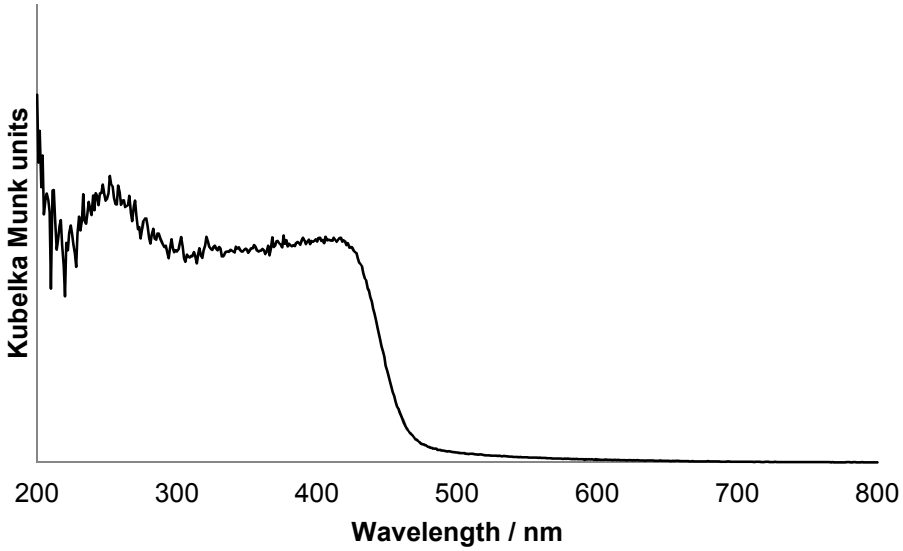

Figure S34. UV-vis spectrum of MIL-53-NH_2/NO_2 (**1**). For the measurement, 5wt% of MIL-53-NH_2/NO_2 in $BaSO_4$ was used. Reflectance data were converted with the Kubleka Munk equation: $F(R) = (1-R)^2/ 2R$.

SHG of MIL-53(Al)-NH_2/NO_2 (1) as a function of temperature

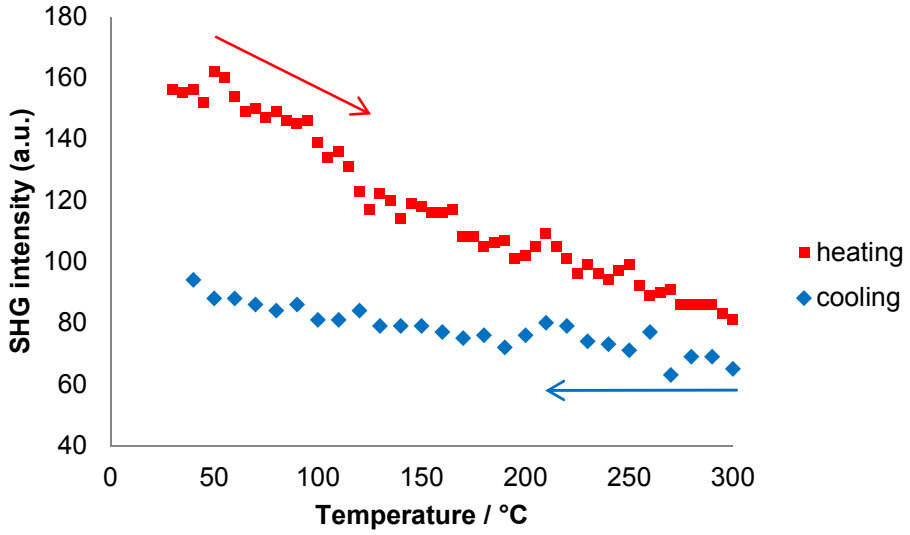

Figure S35. SHG intensity of MIL-53(Al)-NH_2/NO_2 (**1**) during heating and cooling at a rate of 1 °C.min^{-1} under N_2 flow. Between heating and cooling, the temperature was held constant at 300 °C overnight.

Bibliography

(1) Berbenni, V.; Milanese, C.; Bruni, G.; Marini, A. Thermal Decomposition of Gallium Nitrate Hydrate $Ga(NO_3)_3 \times xH_2O$. *J. Therm. Anal. Calorim.* **2005**, *82*, 401–407.

(2) Serra-Crespo, P.; van der Veen, M. A.; Gobechiya, E.; Houthoofd, K.; Filinchuk, Y.; Kirschhock, C. E. A.; Martens, J. A.; Sels, B. F.; De Vos, D. E.; Kapteijn, F.; *et al.* NH_2-MIL-53(Al): A High-Contrast Reversible Solid-State Nonlinear Optical Switch. *J. Am. Chem. Soc.* **2012**, *134*, 8314–8317.

(3) Reinsch, H.; van der Veen, M. A.; Gil, B.; Marszalek, B.; Verbiest, T.; De Vos, D. E.; Stock, N. Structures, Sorption Characteristics, and Nonlinear Optical Properties of a New Series of Highly Stable Aluminum MOFs. *Chem. Mater.* **2013**, *25*, 17–26.

(4) Horcajada, P.; Serre, C.; Grosso, D.; Boissière, C.; Perruchas, S.; Sanchez, C.; Férey, G. Colloidal Route for Preparing Optical Thin Films of Nanoporous Metal-Organic Frameworks. *Adv. Mater.* **2009**, *21*, 1931–1935.

(5) Yang, L.-M.; Vajeeston, P.; Ravindran, P.; Fjellvåg, H.; Tilset, M. Theoretical Investigations on the Chemical Bonding, Electronic Structure, and Optical Properties of the Metal-Organic Framework MOF-5. *Inorg. Chem.* **2010**, *49*, 10283–10290.

(6) Yang, L.-M.; Ravindran, P.; Vajeeston, P.; Tilset, M. Properties of IRMOF-14 and Its Analogues M-IRMOF-14 (M = Cd, Alkaline Earth Metals): Electronic Structure, Structural Stability, Chemical Bonding, and Optical Properties. *Phys. Chem. Chem. Phys. PCCP* **2012**, *14*, 4713–4723.

(7) MUNN, R. W. A General Microscopic Theory of Bulk Second-Harmonic Generation from Molecular Crystals. *Mol. Phys.* **1996**, *89*, 555–569.

(8) Kirtman, B.; Dykstra, C. E.; Champagne, B. Major Intermolecular Effects on Nonlinear Electrical Response in a Hexatriene Model of Solid State Polyacetylene. *Chem. Phys. Lett.* **1999**, *305*, 132–138.

(9) Reis, H.; Papadopoulos, M. G.; Calaminici, P.; Jug, K.; Köster, A. M. Calculation of Macroscopic Linear and Nonlinear Optical Susceptibilities for the Naphthalene, Anthracene and Meta-Nitroaniline Crystals. *Chem. Phys.* **2000**, *261*, 359–371.

(10) Seidler, T.; Stadnicka, K.; Champagne, B. Investigation of the Linear and Second-Order Nonlinear Optical Properties of Molecular Crystals within the Local Field Theory. *J. Chem. Phys.* **2013**, *139*, 114105.

(11) Seidler, T.; Stadnicka, K.; Champagne, B. Second-Order Nonlinear Optical Susceptibilities and Refractive Indices of Organic Crystals from a Multiscale Numerical Simulation Approach. *Adv. Opt. Mater.* **2014**, *2*, 1000–1006.

(12) Dovesi, R.; Orlando, R.; Erba, A.; Zicovich-Wilson, C. M.; Civalleri, B.; Casassa, S.; Maschio, L.; Ferrabone, M.; De La Pierre, M.; D'Arco, P.; *et al.* CRYSTAL14: A Program for the Ab Initio Investigation of Crystalline Solids. *Int. J. Quantum Chem.* **2014**, *114*, 1287–1317.

(13) Seidler, T.; Champagne, B. Which Charge Definition for Describing the Crystal Polarizing Field and the $\chi^{(1)}$ and $\chi^{(2)}$ of Organic Crystals? *Phys. Chem. Chem. Phys.* **2015**, *17*, 19546–19556.

(14) Sekino, H.; Bartlett, R. J. A Linear Response, Coupled-Cluster Theory for Excitation Energy. *Int. J. Quantum Chem.* **1984**, *26*, 255–265.

(15) Seidler, T.; Champagne, B. Second-Order Nonlinear Optical Susceptibilities of Metal–Organic Frameworks Using a Combined Local Field Theory/Charge Embedding Electrostatic Scheme. *J. Phys. Chem. C* **2016**, *120*, 6741–6749.

(16) Frisch, M. J.; Trucks, G. W.; Schlegel, H. B.; Scuseria, G. E.; Robb, M. A.; Cheeseman, J. R.; Scalmani, G.; Barone, V.; Mennucci, B.; Petersson, G. A.; *et al.* Gaussian 09, Revision B.01. *Gaussian 09, Revision B.01, Gaussian, Inc., Wallingford CT*, 2009.

(17) Bru, R.; Walde, P. Product Inhibition of a-Chymotrypsin in Reverse Micelles. *Eur. J. Biochem.* **1991**, *199*, 95–103.